ARTICLE IN PRESS

Mechanical Systems and Signal Processing xxx (xxxx) xxx

FISEVIER

Contents lists available at ScienceDirect

Mechanical Systems and Signal Processing

journal homepage: www.elsevier.com/locate/ymssp



A Scaled Spherical Simplex Filter (S3F) with a decreased n + 2 sigma points set size and equivalent 2n + 1 Unscented Kalman Filter (UKF) accuracy

Konstantinos G. Papakonstantinou*, Mariyam Amir, Gordon P. Warn

Department of Civil and Environmental Engineering, The Pennsylvania State University, University Park, PA 16802, USA

ARTICLE INFO

Article history: Received 3 March 2020 Received in revised form 31 July 2020 Accepted 7 November 2020 Available online xxxx

Keywords:
Unscented Kalman Filter
Sigma points
Sequential probabilistic inference
State estimation
Parameter identification
Online nonlinear filtering

ABSTRACT

The computational efficiency of a sampling based nonlinear Kalman filtering process is mainly conditional on the number of sigma/sample points required by the filter at each time step to effectively quantify statistical properties of related states and parameters. Efficaciously minimizing the needed number of points would therefore have important implications, especially for large n-dimensional nonlinear systems. A set of minimum number of n + 1 sigma points is necessary in each filtering application in order to provide mean and nonsingular covariance estimates. Incorporating additional sigma points than this minimum set improves the accuracy of the estimates and can take advantage of a richer information content that can possibly exist, but at the same time increases the computational demand. To this end, by adding one more sigma point to this minimum set, and assigning general, well defined weights and scaling factors, a new Scaled Spherical Simplex Filter (S3F) with n + 2 sigma points set size is presented in this work, and it is theoretically proven that it can practically achieve in all cases the same accuracy and numerical stability as the typical 2n + 1 sigma points Unscented Kalman Filter (UKF), with almost 50% less computational requirements. A comprehensive study of the suggested filter is presented, including detailed derivations, theoretical examples and numerical results, demonstrating the efficiency, robustness, and accuracy of the S3F.

© 2020 Elsevier Ltd. All rights reserved.

1. Introduction

System identification in the form of dynamic states and parameters inference through available measurements plays an important role for condition assessment, performance prediction, and adaptive control, among others [1,2,3,4]. This work focuses on sigma points based nonlinear Kalman filtering, a time domain, model-based, Bayesian probabilistic technique that can tackle difficult problems of a broad range in a unified formulation, such as linear and nonlinear systems, dual state estimation and parameter identification, linear and/or nonlinear observation equations, online estimations, and sparse measurement data. The Kalman Filter [5] is well known to provide unbiased, minimum variance optimal estimates of the state vector for linear dynamic systems and is widely used in numerous relevant applications. In nonlinear cases however, either as they emerge due to the need for parameters estimation or due to inherent nonlinearities, one of the most popular filters that can be employed, with a long history, is the Extended Kalman Filter (EKF), e.g. [6]. Going beyond the first-order approximations and gradient evaluation requirements in EKF, other nonlinear filtering alternatives have been developed, such as the

E-mail address: kpapakon@psu.edu (K.G. Papakonstantinou).

https://doi.org/10.1016/j.ymssp.2020.107433

0888-3270/© 2020 Elsevier Ltd. All rights reserved.

^{*} Corresponding author.

Unscented Kalman Filter (UKF) [7] and the Particle Filter (PF) [8], among others. In the PF a large number of particles is probabilistically sampled, while in the UKF a predefined set of sigma points is deterministically obtained, in order to eventually quantify the final output statistics. The uncertainty quantification and propagation accuracy and effectiveness attained through a predefined set of sigma points, as in the case of UKF, makes sigma point based filters a viable option in many settings, from a computational perspective [9].

Consequently, numerous researches have been dedicated regarding appropriate sigma points selection, to capture statistical properties of the prior distribution. A symmetric set of 2n + 1 sigma points for UKF has been derived by Julier and Uhlmann and co-workers [10,11,12], to capture the mean and covariance of a n-dimensional random variable following any distribution, and the first three moments for any symmetric distribution, such as the Gaussian one. By increasing the number of sigma points, higher order accuracy can be achieved, as for example in skewed/third moment approaches, conjugate Unscented Transform or higher order filters [13,14,15], albeit by also drastically increasing the computational demand of the filtering process. Since the computational cost of the filtering methodology is proportional to the number of sigma/sample points, there is a strong incentive to minimize the number of points required for uncertainty propagation, especially for computationally expensive models.

Along these lines, a minimum-skew simplex sigma points filter is introduced by Julier and Uhlmann [16], utilizing n + 2points to match the first two moments and to minimize third moment (skew) errors for a *n*-dimensional random variable, where n + 1 points form the vertices of a simplex. In the suggested approach in [16], however, the spread of the points increases exponentially with the state-space dimension, resulting in potential numerical stability problems even for relatively low dimensionality. Julier [17] introduced an alternate strategy for the n + 2 sigma points selection and transformation, named as spherical simplex Unscented Transform, where n + 1 points are now located on a hypersphere with radius proportional to \sqrt{n} . In both [16,17], the sigma points are asymmetrically distributed about the origin, and therefore some symmetric distribution higher moment effects, especially for the skew and the other odd moments, are not captured now by the sigma points. To be able to limit the spread of the sigma points to some extent, in order to utilize the approach in [16] which can minimize third moment errors, the scaled Unscented Transformation is presented by Julier in [18], through the introduction of the scaling parameters α and β . The scaling factor α determines the spread of the sigma points and can suppress higher moments errors, whereas the scaling factor β is used to incorporate potential distribution information relating to its 4th moments. This scaled transformation approach has been eventually formalized by Wan and van der Merwe in [19,20] for the 2n+1 sigma points UKF [10,11,12], and a robust, general methodology is presented for appropriate sigma points selection, weight allocations, and the implementation of the scaling factors α and β . The UKF version in [19,20] is currently the most popular UKF version and it is considered as the standard, state-of-the-art implementation. In this work, we are revisiting these issues and we are formally introducing and generally formalizing the Scaled Spherical Simplex Filter (S3F), which, as we prove, combines all the best attributes of the previous approaches and can achieve an equivalent accuracy and numerical stability with the state-of-the-art 2n + 1 UKF, for all distribution cases, despite using a decreased n + 2 sigma points set size.

The 2n + 1 UKF version is currently widely used and has proven successful in a diverse range of applications for nonlinear systems, because of its ease of implementation, accuracy, computational stability, and efficiency. Only some notable exemplifying works are mentioned here, with more emphasis on structural mechanics applications. The UKF implementation for softening single degree-of-freedom structural systems is shown by Mariani and Ghisi [21], while Wu and Smyth [22] applied the filter for online parametric system identification of hysteretic models with degradation and pinching. Cheng and Feng [23] utilized large-scale experimental and actual field data for two- and three-span bridges, while Chatzi et al. [24] employed the UKF to obtain the most relevant hysteretic model based on the available experimental data. A parallel UKF implementation is discussed in Azam et al. [25], and Omrani et al. [26] applied the UKF to identify the inelastic seismic response of a single-story building. Xie and Feng [27] applied an iterative UKF version for nonlinear system identification, while in Song and Dyke [28] real-time hysteretic model updating of an experimental shear-type steel structure is shown. Papakonstantinou and Shinozuka [29] used UKF outside a traditional dynamic context, for parameter optimization of a computational model in an inverse setting, while Schenkendorf and Mangold [30] presented an online model selection approach based on UKF. Asgarieh et al. [31] applied UKF for nonlinear identification of a seven-story shear wall building, and Al-Hussein and Haldar [32] applied the UKF in applications with unknown inputs. Kontoroupi and Smyth [33] used UKF for online noise identification in joint state and parameter estimation problems, and Chatzis and Chatzi [34] suggested a discontinuous UKF to tackle problems related to observability and identifiability [35] in non-smooth dynamic problems. Astroza et al. [36,37] integrated the UKF with high-fidelity mechanics-based nonlinear finite elements, to estimate unknown material parameters in frame-type structures, Erazo and Hernandez [38] thoroughly compared different filter types for damage assessment, and in Olivier and Smyth [39,40] various nonlinear filters are explored and compared. The impact load and its location are identified by Yan et al. [41] using UKF, and in [42] Song suggested a UKF approach for joint input-state-parameter estimation. Calabrese et al. [43] investigated constrained approaches for UKF, Dertimanis et al. and Lei et al. [44,45] devised UKF schemes for the identification of nonlinear systems and unknown inputs, and Song et al. [46] proposed an adaptive UKF version for model updating and noise identification. Other UKF applications can also be seen in relation to simultaneous localization and mapping (SLAM), robotics, target tracking, autonomous vehicles, dynamic positioning, image processing, and many more. Lastly, among various other applications, the filters can be directly integrated with the recently introduced, flexible, fully parametrized, state-space based hysteretic finite element models in Amir et al. [47,48,49], as presented in Amir et al. [50], and can be also combined with Partially Observable Markov Decision Processes (POMDP) techniques for optimal stochastic control [51,52,53,54].

Motivated by the numerous UKF applications in multiple scientific and engineering fields, the objective of the present work is to formally introduce the Scaled Spherical Simplex Filter (S3F) that can be unrestrictedly utilized in all general applications where UKF can be used, while achieving in all cases an equivalent accuracy and numerical stability for all distribution types, however, with a ~50% reduced computational effort. This is achieved through a reduced sigma points uncertainty propagation mechanism, requiring only n + 2 weighted sigma points, in contrast to the 2n + 1 used in the typical Unscented Transformation. The relevant derivations and the resulting S3F development are discussed in detail and a general, straightforward approach is presented for the selection of the sigma points and their associated weights. The minimum possible number of sigma points needed to provide mean and nonsingular covariance estimates is n + 1, but such a filter cannot achieve the same order of accuracy and robustness as the UKF. By adding one more sigma point to this minimum set, and assigning well defined weights and scaling factors, the suggested n + 2 sigma points S3F can instead preserve all the important features of the UKF. Detailed theoretical proofs are provided to indeed demonstrate that the suggested S3F with appropriate scaling factors can practically achieve the same UKF accuracy of third moment for symmetric prior distributions, such as the Gaussian ones, and second moment in general. Several theoretical examples are also shown, by comparing the estimated mean and covariance outputs of nonlinear functions, assuming bivariate input cases described by correlated Gaussian and lognormal random variables, as well as an arbitrarily defined joint density function. Finally, numerical examples with increasing level of complexity are presented, to showcase the capabilities and advantages of the suggested approach, for problems associated with dual state and parameter estimation, considering systems with hysteresis, sparsity of measurements, large observation and input noises, and time-variant and invariant parameters, among others.

2. Uncertainty propagation and sequential probabilistic inference

Sequential probabilistic inference in the context of this paper is the problem of estimating the hidden states of a nonlinear dynamic system given a set of noisy and sparse observations. Representing the system as the simplest dynamic Bayesian network in a first order hidden Markov model format with continuous states, as in Fig. 1, enables the use of Bayesian estimation algorithms which recursively update the system state posterior density as new observations become available. The hidden system state \mathbf{x} in Fig. 1, having an initial distribution $p(\mathbf{x}_0)$, evolves over time according to the conditional probability density $p(\mathbf{x}_k|\mathbf{x}_{k-1})$, with k being the discrete time index. The observed data \mathbf{u}_k are conditionally independent given the system state and follow the probability density function $p(\mathbf{u}_k|\mathbf{x}_k)$. The system dynamics can be also expressed as:

$$\mathbf{x}_k = \mathbf{f}(\mathbf{x}_{k-1}, \mathbf{q}_k, \mathbf{v}_k, \mathbf{\theta}) \; ; \; \mathbf{u}_k = \mathbf{h}(\mathbf{x}_k, \mathbf{r}_k, \mathbf{v}_k, \mathbf{\theta})$$
 (1)

where \mathbf{f} is the nonlinear state transition function, \mathbf{q} is the process noise, \mathbf{v} is the exogenous input, $\mathbf{0}$ is the parameter vector that parametrizes \mathbf{f} and \mathbf{h} , the nonlinear observation function, and \mathbf{r} is the observation noise. The state transition probability density $p(\mathbf{x}_k|\mathbf{x}_{k-1})$ is fully described by \mathbf{f} and $p(\mathbf{q}_k)$, the process noise distribution, and the observation likelihood $p(\mathbf{u}_k|\mathbf{x}_k)$ is fully specified by \mathbf{h} and $p(\mathbf{r}_k)$, the observation noise distribution.

The posterior density $p(\mathbf{x}_k|\mathbf{u}_{1:k})$ of the system state, given all the observations $\mathbf{u}_{1:k} = \{\mathbf{u}_1, \mathbf{u}_2, \dots, \mathbf{u}_k\}$ is the complete sought solution to this inference problem. To recursively update the posterior density in a Bayesian context, the following classical relationship is used:

$$p(\mathbf{x}_k|\mathbf{u}_{1:k}) = \frac{p(\mathbf{u}_k|\mathbf{x}_k)p(\mathbf{x}_k|\mathbf{u}_{1:k-1})}{\int p(\mathbf{u}_k|\mathbf{x}_k)p(\mathbf{x}_k|\mathbf{u}_{1:k-1})d\mathbf{x}_k}$$
(2)

with $p(\mathbf{x}_k|\mathbf{u}_{1:k-1})$ given by propagating the previous posterior $p(\mathbf{x}_{k-1}|\mathbf{u}_{1:k-1})$ in time:

$$p(\mathbf{x}_{k}|\mathbf{u}_{1:k-1}) = \int p(\mathbf{x}_{k}|\mathbf{x}_{k-1})p(\mathbf{x}_{k-1}|\mathbf{u}_{1:k-1})d\mathbf{x}_{k-1}$$
(3)

For linear, Gaussian systems, Kalman derived the closed-form solution of these integral equations, in what is currently well known as the Kalman filter [5]. Unfortunately, for general nonlinear systems, the closed-form solutions to these multi-dimensional integrals are intractable and approximate methods can only be used, such as the Extended Kalman Filter (EKF) [6] and the Unscented Kalman Filter (UKF) [7], among others, where only the conditional mean $\hat{\mathbf{x}}_k = E[\mathbf{x}_k | \mathbf{u}_{1:k}]$ and covariance \mathbf{P}_k are tracked. In the case that the posterior density is a Gaussian distribution, these two moments can fully describe the posterior density.

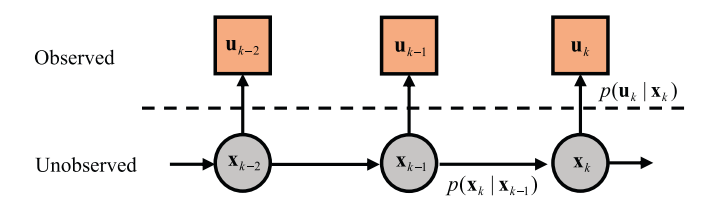


Fig. 1. A hidden Markov model.

The EKF linearizes the nonlinear equations at each step through a Taylor-series expansion and then analytically propagates the associated mean and covariance through the filter. To illustrate, let $\mathbf{x} = \delta \mathbf{x} + \overline{\mathbf{x}}$, where the zero mean random variable $\delta \mathbf{x}$ has the same covariance $\mathbf{P}_{\mathbf{x}\mathbf{x}}$ as \mathbf{x} . Expanding a function \mathbf{f} about $\overline{\mathbf{x}}$ results in:

$$\mathbf{y} = \mathbf{f}(\mathbf{x}) = \mathbf{f}(\overline{\mathbf{x}}) + \nabla \mathbf{f} \delta \mathbf{x} + \frac{1}{2} \nabla^2 \mathbf{f} \delta \mathbf{x}^2 + \frac{1}{3!} \nabla^3 \mathbf{f} \delta \mathbf{x}^3 \dots \tag{4}$$

where $\nabla^i \mathbf{f} \delta \mathbf{x}^i$ is the i^{th} term in the multidimensional Taylor series, as explained in the subsequent sections and expanded in Eq. (9). The mean and covariance used in the EKF are obtained by a first and second moment approximation, respectively, as:

$$\overline{\mathbf{f}(\mathbf{x})} = \overline{\mathbf{y}} \approx \mathbf{f}(\overline{\mathbf{x}}), \ \mathbf{P}_{\mathbf{w}} \approx \nabla \mathbf{f} \mathbf{P}_{\mathbf{x} \mathbf{x}} \nabla \mathbf{f}^{T}$$
 (5)

The nature of this approximation often introduces significant errors and leads to poor performance of the filter in meaning-fully nonlinear problems.

2.1. The Unscented Transformation for UKF

Assuming a n-dimensional random variable, \mathbf{c} , with zero mean, $\mathbf{0}$, and identity covariance, \mathbf{I} , any n-dimensional random variable \mathbf{x} with mean $\overline{\mathbf{x}}$ and covariance $\mathbf{P}_{\mathbf{xx}}$ can be obtained by the affine transformation $\mathbf{x} = \overline{\mathbf{x}} + \sqrt{\mathbf{P}_{\mathbf{xx}}}\mathbf{c}$. Consequently, without loss of generality, the UKF sigma points and weights can be first derived in the c-space and then translated to the x-space. The standard UKF uses a 2n+1 symmetrical set of sigma points, as illustrated in Fig. 2 for a 3-dimensional state-space, i.e. n=3, that are identified by solving a system of moment equations, and are appropriately placed and weighted so as to completely capture the mean and covariance of \mathbf{x} . By slightly reformulating the expressions by Wan and van der Merwe [19], the sigma points \mathbf{X}_i for i=[0,1,...,2n] and the corresponding weights W_i for a scaled UKF are given as:

$$\mathbf{X}_{0} = \overline{\mathbf{x}}
\mathbf{X}_{i} = \overline{\mathbf{x}} + (\alpha \sqrt{n}) \left(\sqrt{\mathbf{P}_{\mathbf{x}\mathbf{x}}} \right)_{i-column} \qquad i = 1, ..., n
\mathbf{X}_{i} = \overline{\mathbf{x}} - (\alpha \sqrt{n}) \left(\sqrt{\mathbf{P}_{\mathbf{x}\mathbf{x}}} \right)_{i-column} \qquad i = n + 1, ..., 2n
W_{0}^{(m)} = 1 - \frac{1}{\alpha^{2}}
W_{0}^{(c)} = 1 - \frac{1}{\alpha^{2}} + (1 - \alpha^{2} + \beta)
W_{i}^{(m)} = W_{i}^{(c)} = \frac{1}{2\alpha^{2}n} \qquad i = 1, ..., 2n$$
(6)

where the superscripts (m) and (c) stand for mean and covariance respectively, and $\alpha\sqrt{n}$ is the radius of the hypersphere where the sigma points in the c-space are distributed. Hence, the value of α determines the spread of the sigma points, and the scaling parameter β incorporates prior knowledge of the distribution \mathbf{x} , as also explained subsequently. The set of points propagates through the function $\mathbf{y} = \mathbf{f}(\mathbf{x})$ to obtain a new set of sigma points \mathbf{Y}_i , which are then employed to evaluate the updated mean and covariance of the transformed random variable \mathbf{y} as follows:

$$\mathbf{Y}_{i} = \mathbf{f}(\mathbf{X}_{i})$$

$$\mathbf{\overline{y}} = \sum_{i=0}^{2n} W_{i}^{(m)} \mathbf{Y}_{i} \quad ; \quad \mathbf{P}_{yy} = \sum_{i=0}^{2n} W_{i}^{(c)} [\mathbf{Y}_{i} - \mathbf{\overline{y}}] [\mathbf{Y}_{i} - \mathbf{\overline{y}}]^{T}$$
(7)

where \overline{y} and P_{yy} are the estimated mean and covariance of the transformed random variable y.

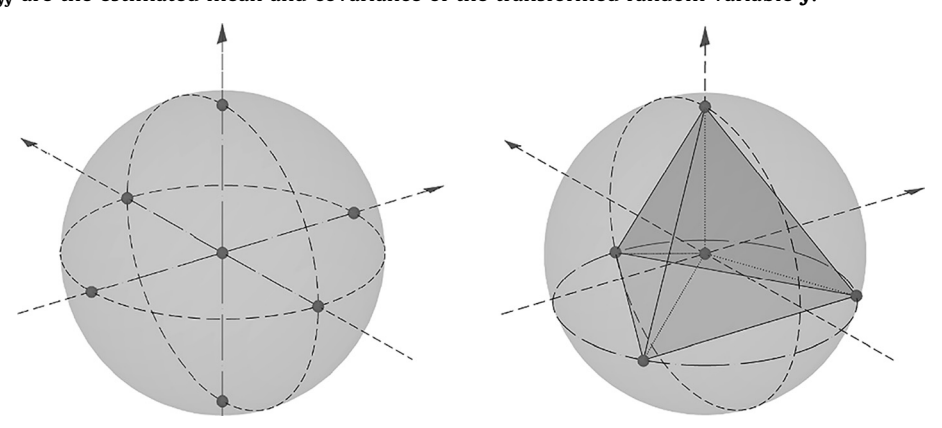


Fig. 2. Sigma points locations on a sphere of radius $\alpha\sqrt{3}$, at the 3-dimensional c-space, for both UKF (left) and S3F (right).

3. The Scaled Spherical Simplex Filter (S3F)

This section presents in detail the general S3F derivations and implementation, and analyzes the selection strategy for the asymmetric sigma points, their associated weights, and the effect of the scaling factors. Comparisons with respect to Taylor series expansion and the 2n + 1 Unscented Transformation scheme of the UKF are provided, and lastly the overall recursive filter estimation method is shown.

Keeping the same notation as in Eq. (4), it can be proved that the mean and covariance of a scaled random variable **x** through a function **f**, with the scaling parameter α , can be expanded as [7.18]:

$$\overline{\mathbf{f}(\mathbf{x})} = \overline{\mathbf{y}} = \mathbf{f}(\overline{\mathbf{x}}) + \frac{1}{2} \nabla^{2} \mathbf{f} \ E[\delta \mathbf{x}^{2}] + \frac{1}{6} \nabla^{3} \mathbf{f} \ \alpha E[\delta \mathbf{x}^{3}] + \dots
\mathbf{P}_{\mathbf{y}\mathbf{y}} = \nabla \mathbf{f} \ \mathbf{P}_{\mathbf{x}\mathbf{x}} \nabla \mathbf{f}^{T} + \alpha \frac{1}{2} \left(\nabla^{2} \mathbf{f} \ E[\delta \mathbf{x}^{2} \delta \mathbf{x}^{T}] \nabla \mathbf{f}^{T} + \nabla \mathbf{f} \ E[\delta \mathbf{x} \delta \mathbf{x}^{2T}] \nabla^{2} \mathbf{f}^{T} \right)
+ \alpha^{2} \frac{1}{4} \nabla^{2} \mathbf{f} \left(E[\delta \mathbf{x}^{2} \delta \mathbf{x}^{2T}] - E[\delta \mathbf{x}^{2}] E[\delta \mathbf{x}^{2}]^{T} \right) \nabla^{2} \mathbf{f}^{T}
+ \alpha^{2} \frac{1}{6} \left(\nabla^{3} \mathbf{f} \ E[\delta \mathbf{x}^{3} \delta \mathbf{x}^{T}] \nabla \mathbf{f}^{T} + \nabla \mathbf{f} \ E[\delta \mathbf{x} \delta \mathbf{x}^{3T}] \nabla^{3} \mathbf{f}^{T} \right) + \dots$$
(8)

where ∇ is the first-order gradient in the form of a row-vector, $\nabla^k \mathbf{f}$ gives the k^{th} order gradient of the function \mathbf{f} , where ∇^k is a row-vector of size n^k consisting of all possible k^{th} order gradients for a n-dimensional system, obtained through the Kronecker product of ∇ performed k-times, $\delta \mathbf{x}$ is a column vector of size n, such that the i^{th} element with $i \in [1, ..., n]$ is given as $\delta x_i = x_i - E[x_i]$, $\delta \mathbf{x}^k$ is the column vector of size n^k obtained by the k-times Kronecker product of vector $\delta \mathbf{x}$, and $E[\delta \mathbf{x}^l \delta \mathbf{x}^{mT}]$ is the $(l+m)^{th}$ central moment of \mathbf{x} , arranged in the appropriate matrix of size (n^l, n^m) , where superscript T represents vector/matrix transpose. Mathematically, all the terms can be thus expressed as:

$$\nabla = \left\{ \frac{\partial}{\partial x_{1}} \frac{\partial}{\partial x_{2}} \cdots \frac{\partial}{\partial x_{n}} \right\} ; \quad \nabla^{k} \mathbf{f} = \underbrace{\nabla \otimes \nabla \cdots \otimes \nabla}_{k \text{ times}} \otimes \mathbf{f} \Big|_{\mathbf{x} = \overline{\mathbf{x}}}$$

$$= \left\{ \frac{\partial \nabla^{k-1}}{\partial x_{1}} \frac{\partial \nabla^{k-1}}{\partial x_{2}} \cdots \frac{\partial \nabla^{k-1}}{\partial x_{n}} \right\} \otimes \mathbf{f} \Big|_{\mathbf{x} = \overline{\mathbf{x}}} ; \quad \delta \mathbf{x} = \left\{ \begin{array}{c} \delta x_{1} \\ \vdots \\ \delta x_{n} \end{array} \right\}$$

$$\delta \mathbf{x}^{k} = \underbrace{\delta \mathbf{x} \otimes \delta \mathbf{x} \cdots \otimes \delta \mathbf{x}}_{k \text{ times}} = \left\{ \begin{array}{c} \delta x_{1} \delta \mathbf{x}^{k-1} \\ \vdots \\ \delta x_{n} \delta \mathbf{x}^{k-1} \end{array} \right\} ; \quad k \in 1, 2, \cdots$$

$$\delta \mathbf{x}^{l} \delta \mathbf{x}^{mT} = \underbrace{\left\{ \delta \mathbf{x} \otimes \cdots \otimes \delta \mathbf{x} \right\}}_{l \text{ times}} \underbrace{\left\{ \delta \mathbf{x} \otimes \cdots \otimes \delta \mathbf{x} \right\}}_{m \text{ times}} ; \quad l, m \in 0, 1, 2, \cdots$$

$$(9)$$

where \otimes is the Kronecker product. Since the UKF set of sigma points captures only the first two moments of the random variable \mathbf{x} , the scaling factor α , also seen in Eq. (6), is required to suppress the errors present in the third and higher moments. As such, the estimations in Eq. (8) are, for any nonlinear function, accurate to the second moment in general, and to the third moment for symmetric priors and symmetric sigma points sets, due to odd moments being zero in both cases.

To reduce the number of used sigma points in Eqs. (6)-(7), which are the ones that dictate the computational cost of the filter for a given n-dimensional system, an alternative filter implementation is suggested in this work, named as the Scaled Spherical Simplex Filter (S3F). Fewer than n+1 points in n-dimensions provide a singular covariance, since the points will always lie on a subspace of less than n-dimensions. As a result, the minimum set of sigma points that can be used by any filter of this kind forms a simplex of n+1 vertices. In order to preserve important features of the classical UKF implementation, one more central point is added to the minimum points set, to take advantage of the scaling parameters α and β , and just as in the scaled UKF case, the rest of the points can be then placed on a hypersphere of radius $\alpha \sqrt{n}$ in the c-space with zero mean and identity covariance matrix, as mentioned earlier. Apart from being at equal distance from the origin, the n+1 points that form the simplex are also equidistant from each other in this suggested formation. In Fig. 2, the sigma points locations in the c-space for the UKF and the S3F filters can be observed and compared.

Similar to Eqs. (6)-(7), the S3F evaluates sigma points X_i in the original space, which are then utilized to estimate the mean and covariance of the output distribution. Therefore, equivalently to the UKF case, the uncertainty quantification and propagation is expressed as:

$$\mathbf{X}_{i} = \overline{\mathbf{x}} + \left(\sqrt{\mathbf{P}_{xx}}\mathbf{C}\right)_{i} \text{ for } i \in [0, 1, 2, ..., n+1]
\mathbf{Y}_{i} = \mathbf{f}[\mathbf{X}_{i}]
\overline{\mathbf{y}} = \sum_{i=0}^{n+1} W_{i}\mathbf{Y}_{i}
\mathbf{P}_{yy} = \sum_{i=0}^{n+1} W_{i}[\mathbf{Y}_{i} - \overline{\mathbf{y}}][\mathbf{Y}_{i} - \overline{\mathbf{y}}]^{T} + (1 - \alpha^{2})[\mathbf{Y}_{0} - \overline{\mathbf{y}}][\mathbf{Y}_{0} - \overline{\mathbf{y}}]^{T}$$
(10)

where \mathbf{C} is a matrix of n+2 sigma points in the c-space, shown in detail in Eq. (12), and W_i are the associated weights, for which the derivations can be seen subsequently. Note that a term related to $(1-\alpha^2)$ is present in the covariance estimate, to properly account for the scaled transformation $\mathbf{f}[\overline{\mathbf{x}} + \alpha(\mathbf{x} - \overline{\mathbf{x}})]$ and to achieve a similar scaling effect in the mean and covariance estimates as in the Taylor series expansion of Eq. (8) [18].

3.1. The Scaled Spherical Simplex Unscented Transformation

The Scaled Spherical Simplex uncertainty propagation mechanism for the S3F is analyzed in detail in this section, following a reduced sigma points Unscented Transform (UT) approach that requires only n + 2 sigma points, in contrast to the typical 2n + 1 points.

3.1.1. Selection of sigma points, weights and scaling factors

As mentioned, a given random variable \mathbf{x} can be transformed to and from a random variable \mathbf{c} , in the standard normal c-space, with zero mean, $\mathbf{0}$, and identity covariance, \mathbf{I} , as follows:

$$\mathbf{c} = \left(\sqrt{\mathbf{P}_{xx}}\right)^{-1} (\mathbf{x} - \overline{\mathbf{x}}) \quad ; \quad \mathbf{x} = \overline{\mathbf{x}} + \sqrt{\mathbf{P}_{xx}} \mathbf{c}$$
 (11)

In the S3F case, n+2 sigma points are selected, $\mathbf{C} = [\mathbf{C}_0 \dots \mathbf{C}_{n+1}]$, to capture the statistical properties of the random variable \mathbf{c} , where $\mathbf{C}_i = \{c_{1,i} \ c_{2,i} \ \dots \ c_{n,i}\}^T$ is a n-dimensional vector representing the i^{th} sigma point, given $i \in [0,1,\dots,n+1]$. Note that the point \mathbf{C}_0 is located at the center, and the remaining n+1 points form the vertices of the simplex. The sigma points matrix for the n-dimensional system is thus formulated as:

and $W_{i\neq 0}$ gives the same assigned weights for all points except the central one with i = 0. All the weights are determined by:

$$W_{i} = W_{1} = \frac{1}{\alpha^{2}(n+1)} \text{ for } i \in [1, 2, ..., n+1] \quad ; \quad W_{0} = 1 - \frac{1}{\alpha^{2}} \quad ; \quad \sum_{i=0}^{n+1} W_{i} = 1$$
 (13)

and the scaling parameter α appropriately determines the central weight and the spread of the sigma points away from the center, lying again on a hypersphere of radius $\alpha\sqrt{n}$, as also shown in Fig. 2 for a three-dimensional space. For the suggested S3F approach, the parameter α should be set to a small positive value (~0.001), as explained subsequently.

3.1.2. Effect of the parameter α . The equivalent accuracy of the 2n+1 UKF and the n+2 S3F is demonstrated in this section, through the parameter α and the scaled Taylor series in Eq. (8). Without loss of generality, a 2-dimensional space is used here for both UKF and S3F cases.

UKF case: For a n = 2 system, the set of 5 (2n + 1) sigma points in the standard normal c-space, as shown in Fig. 3, is obtained as:

$$\mathbf{C}_{2\times5} = \begin{bmatrix} c_{1,0} & c_{1,1} & c_{1,2} & c_{1,3} & c_{1,4} \\ c_{2,0} & c_{2,1} & c_{2,2} & c_{2,3} & c_{2,4} \end{bmatrix} = \begin{bmatrix} 0 & p & 0 & -p & 0 \\ 0 & 0 & -p & 0 & p \end{bmatrix}$$
(14)

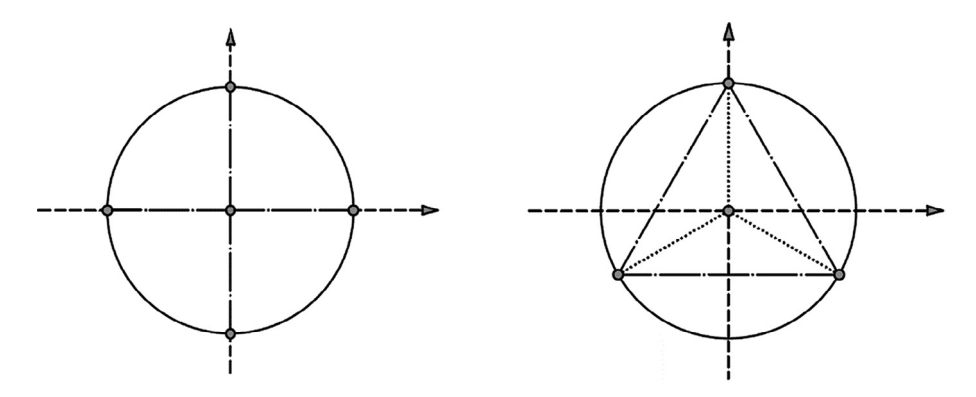


Fig. 3. Sigma points location at the 2-dimensional c-space for both UKF (left) and S3F (right).

where (0,0), (p,0), (0,-p), (-p,0), and (0,p) are the coordinates of the five sigma points, $p=\alpha\sqrt{2}$ and associated weight $W_1=1/(4\alpha^2)$. Based on the selected sigma points, the first moments are obtained as:

$$S_1 = W_0 c_{1,0} + W_1 (c_{1,1} + c_{1,2} + c_{1,3} + c_{1,4}) = W_0(0) + W_1 (p - p) = 0$$

$$S_2 = W_0 c_{2,0} + W_1 (c_{2,1} + c_{2,2} + c_{2,3} + c_{2,4}) = W_0(0) + W_1 (-p + p) = 0$$
(15)

Thus, accurately matching the standard normal space zero mean. The second moments are similarly obtained as:

$$S_{11} = W_0 c_{1,0}^2 + W_1 \left(c_{1,1}^2 + c_{1,2}^2 + c_{1,3}^2 + c_{1,4}^2 \right) = W_0(0) + \frac{1}{4\alpha^2} \left(\left(\alpha \sqrt{2} \right)^2 + \left(-\alpha \sqrt{2} \right)^2 \right) = 1$$

$$S_{22} = W_0 c_{2,0}^2 + W_1 \left(c_{2,1}^2 + c_{2,2}^2 + c_{2,3}^2 + c_{2,4}^2 \right) = W_0(0) + \frac{1}{4\alpha^2} \left(\left(-\alpha \sqrt{2} \right)^2 + \left(\alpha \sqrt{2} \right)^2 \right) = 1$$

$$S_{12} = W_0 c_{1,0} c_{2,0} + W_1 \left(c_{1,1} c_{2,1} + c_{1,2} c_{2,2} + c_{1,3} c_{2,3} + c_{1,4} c_{2,4} \right) = W_0(0) + W_1 \left(4(\alpha \sqrt{2})(0) \right) = 0$$

$$(16)$$

Hence, the condition for identity covariance matrix in the standard normal space is also satisfied. In addition, due to the symmetry of the sigma points all the odd moments are zero, and the fourth moments can be computed similarly as:

$$S_{1111} = W_0 c_{1,0}^4 + W_1 \left(c_{1,1}^4 + c_{1,2}^4 + c_{1,3}^4 + c_{1,4}^4 \right) = W_0(0) + \frac{1}{4\alpha^2} \left(\left(\alpha \sqrt{2} \right)^4 + \left(-\alpha \sqrt{2} \right)^4 \right) = 2\alpha^2 \approx 0 \tag{17}$$

with α being a small positive value (\sim 0.001). Accordingly, any k^{th} moment is proportional to $\alpha^{(k-2)}$ for k=[4,6,8...], and hence all higher moment terms become negligible with α being small.

Overall, the UKF sigma points are accurately capturing the first two moments in the standard normal space, and consequently in the original space as well, while suppressing the errors in the higher moment terms by applying the appropriate scaling factor α . They are thus offering second moment accuracy for any given prior distribution and third moment accuracy for symmetric prior distribution, due to their own symmetry.

S3F case: For the S3F in a 2-dimensional space case, as shown in Fig. 3, the \mathbf{C} matrix, consisting of four sigma points now (n + 2), is obtained based on Eq. (12) as:

$$\mathbf{C}_{2\times 4} = \begin{bmatrix} c_{1,0} & c_{1,1} & c_{1,2} & c_{1,3} \\ c_{2,0} & c_{2,1} & c_{2,2} & c_{2,3} \end{bmatrix} = \begin{bmatrix} 0 & -q_1 & q_1 & 0 \\ 0 & -\frac{q_2}{2} & -\frac{q_2}{2} & q_2 \end{bmatrix} \qquad ; \qquad \text{where } W_1 = \frac{1}{3\alpha^2}; \ q_1 = \alpha\sqrt{\frac{3}{2}}; \ q_2 = \alpha\sqrt{2} \tag{18}$$

and similar to the UKF the radius of the circle in this case is again given by $\alpha\sqrt{2}$. To verify the equivalent UKF accuracy of the S3F methodology, the first moments based on the selected sigma points are now obtained as:

$$S_{1} = W_{0}c_{1,0} + W_{1}(c_{1,1} + c_{1,2} + c_{1,3}) = W_{0}(0) + W_{1}(-q_{1} + q_{1}) = 0$$

$$S_{2} = W_{0}c_{2,0} + W_{1}(c_{2,1} + c_{2,2} + c_{2,3}) = W_{0}(0) + W_{1}\left(-\frac{q_{2}}{2} - \frac{q_{2}}{2} + q_{2}\right) = 0$$
(19)

while the second moments are given as:

$$S_{11} = W_0 c_{1,0}^2 + W_1 \left(c_{1,1}^2 + c_{1,2}^2 + c_{1,3}^2 \right) = W_0(0) + \frac{1}{3\alpha^2} \left(\left(-\alpha \sqrt{\frac{3}{2}} \right)^2 + \left(\alpha \sqrt{\frac{3}{2}} \right)^2 \right) = 1$$

$$S_{22} = W_0 c_{2,0}^2 + W_1 \left(c_{2,1}^2 + c_{2,2}^2 + c_{2,3}^2 \right) = W_0(0) + \frac{1}{3\alpha^2} \left(\left(-\alpha \sqrt{\frac{1}{2}} \right)^2 + \left(\alpha \sqrt{\frac{1}{2}} \right)^2 + \left(\alpha \sqrt{\frac{1}{2}} \right)^2 \right) = 1$$

$$S_{12} = W_0 c_{1,0} c_{2,0} + W_1 \left(c_{1,1} c_{2,1} + c_{1,2} c_{2,2} + c_{1,3} c_{2,3} \right) = W_0(0) + W_1 \left(\frac{q_1 q_2}{2} - \frac{q_1 q_2}{2} + 0 \right) = 0$$

$$(20)$$

Mechanical Systems and Signal Processing xxx (xxxx) xxx

satisfying both zero mean and identity covariance matrix conditions with this reduced set of sigma points. However, contrary to the UKF, due to the asymmetric distribution of points here, the odd moments are non-zero, and third and fourth moments are thereby evaluated as:

$$\begin{split} S_{111} &= W_0 c_{1,0}^3 + W_1 \left(c_{1,1}^3 + c_{1,2}^3 \right) = W_0(0) + W_1 \left(\left(-q_1 \right)^3 + \left(q_1 \right)^3 \right) = 0 \\ S_{122} &= W_0 c_{1,0} c_{2,0}^2 + W_1 \left(c_{1,1} c_{2,1}^2 + c_{1,2} c_{2,2}^2 \right) = W_0(0) + W_1 \left(-\frac{q_1 q_2^2}{4} + \frac{q_1 q_2^2}{4} \right) = 0 \\ S_{222} &= W_0 c_{2,0}^3 + W_1 \left(c_{2,1}^3 + c_{2,2}^3 + c_{2,3}^3 \right) = W_0(0) + \frac{1}{3\alpha^2} \left(\left(-\frac{\alpha\sqrt{2}}{2} \right)^3 + \left(-\frac{\alpha\sqrt{2}}{2} \right)^3 + \left(\alpha\sqrt{2} \right)^3 \right) = \frac{\alpha}{\sqrt{2}} \\ S_{112} &= W_0 c_{1,0} c_{2,0}^2 + 2 W_1 c_{1,1}^2 c_{2,1} = W_0(0) + 2 \frac{1}{3\alpha^2} \left(\alpha\sqrt{\frac{3}{2}} \right)^2 \left(-\frac{\alpha\sqrt{2}}{2} \right) = -\frac{\alpha}{\sqrt{2}} \\ S_{1111} &= W_0 c_{1,0}^4 + W_1 2 c_{1,1}^4 = W_0(0) + \frac{1}{3\alpha^2} (2) \left(\alpha\sqrt{\frac{3}{2}} \right)^4 = \frac{3\alpha^2}{2} \quad \text{(One of the 4$^{th} moments)} \end{split}$$

Accordingly, any k^{th} moment is proportional to $\alpha^{(k-2)}$ for k = [4, 6, 8...], and proportional to $\alpha^{(k-2)}$ or 0 for k = [3, 5, 7...] because some of the odd moments are exactly zero, due to the sigma points symmetry about one axis. Therefore, all the third and higher moment terms are inherently zero, or become zero due to the small value of the scaling factor α .

Thus, similar to the UKF and the scaled Taylor expansion in Eq. (8), the S3F sigma points also offer up to second moment accuracy for any given prior distribution and up to third moment accuracy for any symmetric prior distribution, mainly due to the small value of the scaling factor α , that also nullifies all higher moments effects.

3.1.3. Effect of the parameter β . The effect of the scaling parameter β in the S3F is again similar to that of the UKF [18,19,20], which is to capture some of the fourth moments of the Taylor series expansion. The β parameter can be only included in the covariance term, $\mathbf{P_{w}}$, to approximate the following fourth moment term of the Taylor series at no additional computational effort:

$$\mathbf{A_4} = \frac{1}{4} \nabla^2 \mathbf{f} \left(E[\delta \mathbf{x}^2 \delta \mathbf{x}^{2T}] - E[\delta \mathbf{x}^2] E[\delta \mathbf{x}^2]^T \right) \nabla^2 \mathbf{f}^T$$
(22)

where A_4 is the third term of the Taylor expansion in Eq. (8), without the scaling effects. Since the sigma points transformation only captures the first two prior moments, certain algebraic manipulations are performed to capture the A_4 effect in the final output covariance expression. With $Y_0 = f(\bar{x})$, the following expressions are obtained for the central term:

$$\overline{\boldsymbol{y}} - \boldsymbol{Y}_0 = \left[\boldsymbol{f}(\overline{\boldsymbol{x}}) + \frac{1}{2} \nabla^2 \boldsymbol{f} \ \boldsymbol{E} \big[\delta \boldsymbol{x}^2 \big] + \frac{1}{6} \nabla^3 \boldsymbol{f} \ \boldsymbol{E} \big[\delta \boldsymbol{x}^3 \big] + \ldots \right] - \boldsymbol{f}(\overline{\boldsymbol{x}}) \ = \ \frac{1}{2} \nabla^2 \boldsymbol{f} \ \boldsymbol{E} \big[\delta \boldsymbol{x}^2 \big] + \frac{1}{6} \nabla^3 \boldsymbol{f} \ \boldsymbol{E} \big[\delta \boldsymbol{x}^3 \big] + \ldots \tag{23}$$

$$(\mathbf{Y}_0 - \overline{\mathbf{y}})(\mathbf{Y}_0 - \overline{\mathbf{y}})^T = \frac{1}{4} \nabla^2 \mathbf{f} \ E[\delta \mathbf{x}^2] E[\delta \mathbf{x}^2]^T \nabla^2 \mathbf{f}^T + \dots$$
(24)

Therefore, the central covariance term in Eq. (10) can be further scaled to partially capture fourth moments, and the resulting covariance estimate now becomes:

$$\mathbf{P}_{\mathbf{y}\mathbf{y}} = \sum_{i=0}^{n+1} W_i [\mathbf{Y}_i - \overline{\mathbf{y}}] [\mathbf{Y}_i - \overline{\mathbf{y}}]^T + (1 - \alpha^2) [\mathbf{Y}_0 - \overline{\mathbf{y}}] [\mathbf{Y}_0 - \overline{\mathbf{y}}]^T + \underbrace{\beta [\mathbf{Y}_0 - \overline{\mathbf{y}}] [\mathbf{Y}_0 - \overline{\mathbf{y}}]^T}_{\text{Added for fourth property effects}}$$
(25)

The error in the A_4 and the fourth moment term is thus obtained as:

$$\Delta \mathbf{A} = \mathbf{A_4} - \beta [\mathbf{Y_0} - \overline{\mathbf{y}}] [\mathbf{Y_0} - \overline{\mathbf{y}}]^T \qquad = \frac{1}{4} \nabla^2 \mathbf{f} \left(E \left[\delta \mathbf{x}^2 \delta \mathbf{x}^{2T} \right] - (\beta + 1) E \left[\delta \mathbf{x}^2 \right] E \left[\delta \mathbf{x}^2 \right]^T \right) \nabla^2 \mathbf{f}^T$$
(26)

and β can be determined accordingly to minimize $\Delta \mathbf{A}$, if relevant information is available. For the case of a normal density function, for example, the optimal value of β is 2, since $E[\delta \mathbf{x}^2 \delta \mathbf{x}^{2T}] \approx 3E[\delta \mathbf{x}^2]E[\delta \mathbf{x}^2]^T$. Note that the approximate sign is used herein since not all terms in the matrices satisfy the aforementioned relationship in a general multivariate case. Taking both scaling parameters α and β into account, the modified weights and the posterior mean and covariance matrix are now obtained as:

$$W_{0}^{(m)} = 1 - \frac{1}{\alpha^{2}} \; ; \; W_{0}^{(c)} = 1 - \frac{1}{\alpha^{2}} + (1 - \alpha^{2} + \beta)$$

$$W_{i}^{(m)} = W_{i}^{(c)} = \frac{1}{\alpha^{2}(n+1)}; \qquad i = 1, ..., (n+1)$$

$$\overline{\mathbf{y}} = \sum_{i=0}^{n+1} W_{i}^{(m)} \mathbf{Y}_{i} \; ; \quad \mathbf{P}_{\mathbf{yy}} = \sum_{i=0}^{n+1} W_{i}^{(c)} [\mathbf{Y}_{i} - \overline{\mathbf{y}}]^{T}$$
(27)

Table 1Sigma points selection for UKF and S3F.

UKF	S3F						
Sigma points weights							
$\begin{aligned} W_0^{(m)} &= 1 - \frac{1}{\alpha^2} \\ W_0^{(c)} &= 1 - \frac{1}{\alpha^2} + (1 - \alpha^2 + \beta) \\ W_i^{(m)} &= W_i^{(c)} = \frac{1}{2\alpha^2 n} \qquad i = 1,, 2n \end{aligned}$	$W_0^{(m)} = 1 - \frac{1}{\alpha^2} \ W_0^{(c)} = 1 - \frac{1}{\alpha^2} + (1 - \alpha^2 + \beta)$						
$W_0^{(c)} = 1 - \frac{1}{\alpha^2} + (1 - \alpha^2 + \beta)$	$W_0^{(c)} = 1 - \frac{1}{\alpha^2} + (1 - \alpha^2 + \beta)$						
$W_i^{(m)} = W_i^{(c)} = \frac{1}{2\alpha^2 n}$ $i = 1,, 2n$	$W_i^{(m)} = W_i^{(c)} = \frac{1}{\alpha^2(n+1)}$ $i = 1,, n+1$						

Sigma points for *n*-dimensional random variable \mathbf{x} , with mean $\overline{\mathbf{x}}$ and covariance matrix $\mathbf{P}_{\mathbf{x}\mathbf{x}}$

Value of parameter α is small, for example in the range of 0.01 to 0.0001, and parameter β can be determined based on Eq. (26) or else β =2, if no relevant fourth moment information is available.

where (m) stands for the mean and (c) for the covariance. A concise overview for the final sigma points selection for both scaled UKF and S3F is provided in Table 1.

3.2. S3F without central point: The Spherical Simplex Filter (S2F)

As seen in Table 1, with $\alpha=1$ and $\beta=0$, the central point is no longer used and only the absolute minimum set of n+1 points is now utilized. This is a byproduct of the presented S3F formulation, that leads to the filter variant, referred to here as the *Spherical Simplex Filter* (S2F). The S2F has therefore the exact same logic as the S3F, with the important difference that $W_0^{(n)}=W_0^{(c)}=0$ and the exclusion of the central sigma point. All the relevant equations in Table 1 still apply in this case but the S2F does not necessarily have all of the odd moments equal to zero in the absence of any scaling effects, with $\alpha=1$, because of the asymmetry in the sigma points distribution. As such, S2F exhibits, in general, a lower approximation accuracy in comparison to the UKF and S3F.

3.3. Filtering methodology

The \mathbf{X}_{k-1} sigma points at the $(k-1)^{th}$ time step, selected based on the random variables with mean $\widehat{\mathbf{X}}_{k-1}$ and covariance matrix \mathbf{P}_{k-1} , estimated either through the UKF or the S3F (Table 1), propagate through the function \mathbf{f} of Eq. (1) and the updated mean and covariance can be estimated as:

$$\mathbf{X}_{k|k-1} = \mathbf{f}[\mathbf{X}_{k-1}, \mathbf{v}_k, \boldsymbol{\theta}]$$

$$\widehat{\mathbf{X}}_k^- = \sum_{i=0}^L W_i^{(m)} \mathbf{X}_{i,k|k-1}$$

$$\mathbf{P}_k^- = \sum_{i=0}^L W_i^{(c)} [\mathbf{X}_{i,k|k-1} - \widehat{\mathbf{x}}_k^-] [\mathbf{X}_{i,k|k-1} - \widehat{\mathbf{x}}_k^-]^T + \mathbf{Q}_k$$
(28)

where L=2n for the UKF and L=(n+1) for the S3F, and \mathbf{Q}_k is the process noise covariance for the case of additive zero mean noise \mathbf{q}_k .

To incorporate this effect of the additive process noise, the $\mathbf{X}_{k|k-1}$ sigma points are redrawn based now on the current mean and covariance estimates $(\hat{\mathbf{x}}_k^-, \mathbf{P}_k^-)$, and are subsequently used as inputs in the observation function \mathbf{h} of Eq. (1), in order to calculate the appropriate mean vector and covariance matrices, as:

$$\mathbf{U}_{k|k-1} = \mathbf{h}(\mathbf{X}_{k|k-1}, \mathbf{v}_k, \mathbf{\theta})
\widehat{\mathbf{u}}_k^- = \sum_{i=0}^L W_i^{(m)} \mathbf{U}_{i,k|k-1}
\mathbf{P}_{u_k u_k} = \sum_{i=0}^L W_i^{(c)} \left[\mathbf{U}_{i,k|k-1} - \widehat{\mathbf{u}}_k^- \right] \left[\mathbf{U}_{i,k|k-1} - \widehat{\mathbf{u}}_k^- \right]^T + \mathbf{R}_k
\mathbf{P}_{\mathbf{x}_k u_k} = \sum_{i=0}^L W_i^{(c)} \left[\mathbf{X}_{i,k|k-1} - \widehat{\mathbf{x}}_k^- \right] \left[\mathbf{U}_{i,k|k-1} - \widehat{\mathbf{u}}_k^- \right]^T$$
(29)

where \mathbf{R}_k the observation noise covariance, for the case of additive zero mean noise \mathbf{r}_k . Finally, when an observation \mathbf{u}_k becomes available, the posterior mean $\hat{\mathbf{x}}_k$ and covariance \mathbf{P}_k for this time step are updated through the Kalman gain \mathbf{K}_k , as [20]:

$$\mathbf{K}_{k} = \mathbf{P}_{x_{k}u_{k}}\mathbf{P}_{u_{k}u_{k}}^{-1}$$

$$\mathbf{\hat{x}}_{k} = \mathbf{\hat{x}}_{k}^{-} + \mathbf{K}_{k}(\mathbf{u}_{k} - \mathbf{\hat{u}}_{k}^{-})$$

$$\mathbf{P}_{k} = \mathbf{P}_{k}^{-} - \mathbf{K}_{k}\mathbf{P}_{u_{k}u_{k}}\mathbf{K}_{k}^{T}$$
(30)

4. Theoretical analysis and examples

4.1. Theoretical example 1

In this example, for a given random bivariate input $\mathbf{x} = \begin{cases} x_1 \\ x_2 \end{cases}$, with $\overline{\mathbf{x}} = E[\mathbf{x}] = \begin{cases} \mu_1 \\ \mu_2 \end{cases}$; $\mathbf{P_{xx}} = \begin{bmatrix} m_{11} & m_{12} \\ m_{12} & m_{22} \end{bmatrix}$, the mean and variance of the output random variable, $y = f(\mathbf{x}) = x_1x_2$ is obtained. Two cases are analyzed, first when \mathbf{x} follows a Gaussian distribution (GRV), and second when it is lognormally (LN) distributed. Appropriate moment generating functions are employed to obtain the higher moments required for the analysis herein. Detailed derivations can be seen in the Appendix. Note that for the GRV, all the odd moments of $\delta \mathbf{x} = \mathbf{x} - \overline{\mathbf{x}}$ are zero, while for LN they have non-zero values. The results are summarized in Table 2.

As seen in Table 2, the Taylor series and filter approaches in this example are accurate to the second moment for the mean estimates, and given that the analyzed function has zero 3^{rd} and higher order gradients, the estimated mean coincides with the true mean in all cases and is not dependent on the scaling factors. The obtained variance in the GRV scaled Taylor series case is correct up to the third moment estimates, since the fourth moment terms are suppressed due to the small α value. In the LN case, the scaling effect suppresses the third and higher moment terms in the Taylor series estimate of the variance, thereby resulting in accuracy to the second moment. The complete expressions can be seen in the Appendix. Again, for small α , i.e. 0.001, both UKF and S3F provide the same accuracy, i.e. up to third moment if the prior is symmetric and up to second moment otherwise, while the parameter β partially captures the fourth moment terms. Note that the parameter β is not applicable in the Taylor series expansion of Eq. (8). When no scaling is present, as seen in the S2F case, estimates may diverge in some cases due to the introduced error by the higher moment terms.

4.2. Theoretical example 2

In this example, the mean and variance of a random variable $y=x_2\sin(x_1)$ is obtained, given the joint probability density function $f_{X_1X_2}(x_1,x_2)=\frac{4x_1}{\pi^3}(3x_1+2x_2\pi)$, where $x_1\in[0\ \pi/2]$, $x_2\in[0\ 1]$. The first moments of the input random variables are obtained using the following integrals:

$$\mu_{X_1} = \int_{x_2=0}^{1} \int_{x_1=0}^{\pi/2} x_1 f_{X_1 X_2}(x_1, x_2) dx_1 dx_2 = \frac{17\pi}{48} = 1.1126$$

$$\mu_{X_2} = \int_{x_2=0}^{1} \int_{x_1=0}^{\pi/2} x_2 f_{X_1 X_2}(x_1, x_2) dx_1 dx_2 = \frac{7}{12} = 0.5833$$
(31)

Table 2Comparison of mean and covariance estimates for Gaussian (GRV) and lognormal (LN) distribution cases.

$y = x_1 x_2$	Mean	Variance
Exact (GRV)	$\mu_1 \mu_2 + m_{12}$	$\mu_2^2 m_{11} + 2\mu_1 \mu_2 m_{12} + \mu_1^2 m_{22} + m_{12}^2 + m_{22} m_{11}$
Taylor (Eq.(8)) (GRV)	$\underbrace{\mu_1\mu_2 + m_{12}}_{1^{\text{st}} \& 2^{nd} \text{ moments}}$	$\underbrace{(\mu_2^2 m_{11} + 2\mu_1 \mu_2 m_{12} + \mu_1^2 m_{22})_{2^{\text{nd}} \text{ moments}}}_{+ \alpha^2 \underbrace{(m_{12}^2 + m_{22} m_{11})}_{4^{\text{th}} \text{ moments}}$
Exact (LN)	$\mu_1 \mu_2 + m_{12}$	$\mu_2^2 m_{11} + 2\mu_1 \mu_2 m_{12} + \mu_1^2 m_{22} + (3^{rd} \text{ and higher moments})$. See Appendix
Taylor (Eq. (8)) (LN)	$\mu_1 \mu_2 + m_{12}$	$\mu_2^2 m_{11} + 2\mu_1 \mu_2 m_{12} + \mu_1^2 m_{22} + \alpha \ (3^{\text{rd}} \text{ moments}) + \alpha^2 \ (4^{\text{th}} \text{ moments}) \dots$ See Appendix
UKF	$\mu_1 \mu_2 + m_{12}$	$\mu_2^2 m_{11} + 2\mu_1 \mu_2 m_{12} + \mu_1^2 m_{22} + \beta m_{12}^2 + \alpha^2 m_{12}^2$
S3F	$\mu_1\mu_2+m_{12}$	$\mu_2^2 m_{11} + 2\mu_1 \mu_2 m_{12} + \mu_1^2 m_{22} + \beta m_{12}^2 - \alpha \sqrt{\frac{2\left(m_{11} m_{22} - m_{12}^2\right)}{m_{11}}} \left(m_{11} \mu_2 + m_{12} \mu_1\right) + \frac{\alpha^2}{2} m_{11} m_{22}$
S2F	$\mu_1\mu_2+m_{12}$	$\mu_2^2 m_{11} + 2\mu_1 \mu_2 m_{12} + \mu_1^2 m_{22} - \sqrt{\frac{2(m_{11} m_{22} - m_{12}^2)}{m_{11}}} (m_{11} \mu_2 + m_{12} \mu_1) + \frac{1}{2} m_{11} m_{22}$

For the scaled Taylor series approximation in Eq. (8), higher centralized moments are evaluated as:

$$E\left[\delta x_{1}^{l}\delta x_{2}^{m}\right] = E\left[\left(x_{1} - \mu_{X_{1}}\right)^{l}\left(x_{2} - \mu_{X_{2}}\right)^{m}\right] = \int_{x_{2}=0}^{1} \int_{x_{1}=0}^{\pi/2} \left(x_{1} - \mu_{X_{1}}\right)^{l}\left(x_{2} - \mu_{X_{2}}\right)^{m} f_{X_{1}X_{2}}\left(x_{1}, x_{2}\right) dx_{1} dx_{2}$$

$$(32)$$

where l + m gives the order of the moment. All moments up to fourth order are provided in the Appendix. The true mean and variance of the random variable Y can be obtained as:

$$\mu_{Y} = \int_{x_{2}=0}^{1} \int_{x_{1}=0}^{\pi/2} y f_{X_{1}X_{2}}(x_{1}, x_{2}) dx_{1} dx_{2} = \frac{2(-18 + 13\pi)}{3\pi^{3}}$$

$$\sigma_{Y} = \int_{x_{2}=0}^{1} \int_{x_{1}=0}^{\pi/2} (y - \mu_{Y})^{2} f_{X_{1}X_{2}}(x_{1}, x_{2}) dx_{1} dx_{2} = \frac{15\pi^{6} + 72\pi^{4} - 5,408\pi^{2} + 14,976\pi - 10,368}{72\pi^{6}}$$
(33)

The results for the UKF and S3F transformations, as well as the scaled Taylor series estimates are summarized in Table 3, where the values in the parentheses give the % error for the estimated mean and variance as compared to the exact values. As seen in the table, the Taylor series approximations are slightly different from the exact values, since the scaled Taylor series achieves accuracy up to the second order moment due to the scaling factor α . The S3F with $\alpha = 0.001$, $\beta = 0$ also results in the same mean and variance values with the Taylor expansion, since the exact same effects of suppressing the third and higher moments are included in the S3F. Lastly, the S3F and UKF with $\alpha = 0.001$, $\beta = 2$ provide improved accuracy for the variance estimates, in comparison to the Taylor series and S3F with $\beta = 0$ cases, because the parameter β now partially captures some fourth moments terms as well. As thoroughly explained, the UKF and S3F provide the exact same estimates with the given scaling parameters, for both the mean and variance.

The effect of different scaling factor values for the S3F is further examined in Table 4. The value of β is not affecting the mean, while both α and β are considered for the variance estimate. To control the introduced error by the higher moment terms, the small value of 0.001 should be used for α , and the default value of β = 2 can be generally used for partially capturing the fourth moments, as already indicated in Table 1.

Table 3Comparison of mean and variance estimates for theoretical example 2.

$y = x_2 \sin(x_1)$	Mean	Variance
Exact	0.4911	0.0685
Taylor (Eq.(8)) ($\alpha = 0.001$, $\beta = N/A$)	0.4896 (0.3%)	0.0669 (2.3%)
S3F ($\alpha = 0.001$, $\beta = 0$)	0.4896 (0.3%)	0.0669 (2.3%)
S3F ($\alpha = 0.001$, $\beta = 2$)	0.4896 (0.3%)	0.0691 (0.9%)
UKF ($\alpha = 0.001$, $\beta = 2$)	0.4896 (0.3%)	0.0691 (0.9%)

Table 4The effect of scaling factors on the mean and variance estimates.

$y = x_2 \sin(x_1)$	Mean	Variance
Exact	0.4911	0.0685
S3F (α = 0.001, β = 2)	0.4896 (0.3%)	0.0691 (0.9%)
S2F ($\alpha = 1$, $\beta = 0$)	0.5004 (1.9%)	0.0715 (4.4%)
S3F ($\alpha = 0.001$, $\beta = 10$)	0.4896 (0.3%)	0.0781 (14.0%)
S3F ($\alpha = 1$, $\beta = 10$)	0.5004 (1.9%)	0.0766 (11.8%)

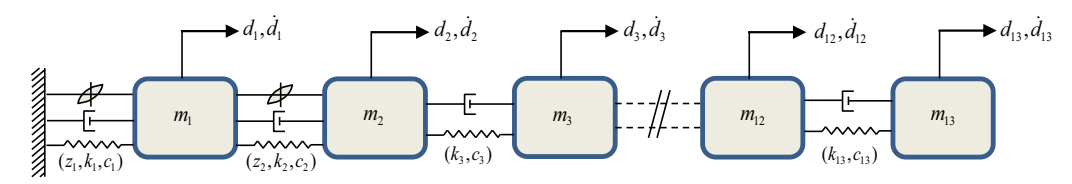


Fig. 4. Nonlinear hysteretic model.

5. Numerical examples

To examine the performance of the presented S3F filter in comparison to the standard UKF implementation, several numerical examples with different levels of complexity are presented, based on a 13-degree of freedom (13-DOF) mass-spring-dashpot nonlinear dynamic system, as illustrated in Fig. 4. For the examples presented here, the first and second DOFs are associated with a Bouc-Wen hysteretic component, as also seen in Fig. 4. The equation of motion and the state-space formulation governing the system dynamics are given similarly to the 3-DOF expressions in [9] and succinctly presented here as:

$$\begin{aligned} \mathbf{M}\ddot{\mathbf{d}} + \mathbf{C}\dot{\mathbf{d}} + \mathbf{K}\mathbf{d} + \mathbf{H}\mathbf{z} &= \mathbf{P}(t) \quad ; \quad \left\{ \begin{matrix} \dot{\mathbf{d}} \\ \ddot{\mathbf{d}} \end{matrix} \right\} = \begin{bmatrix} \mathbf{0} & \mathbf{I} & \mathbf{0} \\ -\mathbf{M}^{-1}\mathbf{K} & -\mathbf{M}^{-1}\mathbf{C} & -\mathbf{M}^{-1}\mathbf{H} \end{bmatrix} \left\{ \begin{matrix} \dot{\mathbf{d}} \\ \dot{\mathbf{d}} \\ \mathbf{z} \end{matrix} \right\} + \left\{ \begin{matrix} \mathbf{0} \\ \mathbf{M}^{-1}\mathbf{P}(t) \end{matrix} \right\} \\ \dot{\theta} &= \left\{ \dot{\mathbf{c}} \quad \dot{\mathbf{k}} \quad \dot{\boldsymbol{\beta}}_{BW} \quad \dot{\boldsymbol{\gamma}}_{BW} \quad \dot{\mathbf{n}}_{BW} \right\}^{T} &= \mathbf{0}, \quad \dot{\mathbf{z}} = f\left(\dot{\mathbf{d}}, \mathbf{z}\right), \\ \dot{z}_{i} &= \dot{d}_{i} - \gamma_{BW_{i}} |z_{i}|^{n_{BW_{i}}} \dot{d}_{i} sgn\left(z_{i}\dot{d}_{i}\right) - \beta_{BW_{i}} |z_{i}|^{n_{BW_{i}}} \dot{d}_{i} \\ \mathbf{x} &= \left\{ \mathbf{d}^{T} \quad \dot{\mathbf{d}}^{T} \quad \mathbf{z}^{T} \quad \boldsymbol{\theta}^{T} \right\}^{T} \end{aligned} \tag{34}$$

where **M**, **C**, **K** are the mass, viscous damping and stiffness matrices respectively, and **H** is a hysteretic matrix associated with the nonlinear DOFs (as all provided in the Appendix), **I** and **0** are identity and null matrices respectively, **d** is the displacement vector, **z** is the vector of the hysteretic component of the relevant displacements, **x** is the overall state-parameter vector to be identified, and **P**(t) is the excitation vector related to the input ground acceleration. The Bouc-Wen parameters, β_{BW} , γ_{BW} and n_{BW} , and all stiffness, t, and damping terms, t, are assumed unknown and have been augmented in the state vector in this case, as seen in Eq. (34), in order to be identified by the filtering process in the dual state and parameter estimation examples presented herein. This dual estimation process, together with the nature of the system dynamics in Eq. (34), constitute the particular examples in this section highly nonlinear.

The dimension of the augmented state-parameter vector \mathbf{x} in Eq. (34) is n = 71, and hence the number of sigma points required for the UKF are 143 (=2n + 1), whereas S3F employs only 73 sigma points (=n + 2) in this case, thereby improving the numerical efficiency by ~50%. A scaled Chi-Chi acceleration record has been used for all examples, as seen in Fig. 5(a), available in the NGA-West2 PEER database [55]. The Heun's (modified Euler's) method is successfully used to solve Eq. (34) in time, after examining its accuracy with a highly accurate (but rather slow) variable-step, implicit, 6th order Adams-Moulton solver.

For illustration purposes, all numbers have been normalized accordingly. All masses are considered known and equal to 0.9. The correct damping and Bouc-Wen parameters are the same for all numerical examples and are summarized in Table 5. The initial stiffness values are also the same for all examples, however different cases are examined with and without time variant values. For all numerical examples, the scaling factors values of $\alpha = 0.001$ and $\beta = 2$ are used, for both UKF and S3F, based on Table 1, unless otherwise specified. For the estimation process, in all the examples, the observation noise and process noise at each time step k are generically assumed to be zero mean Gaussian white noises with $\mathbf{R}_k = \mathbf{R} = 0.003\mathbf{I}$, where \mathbf{I} is the identity matrix of size equal to the number of observed measurements, and \mathbf{Q}_k is assumed to have all its elements zeros, except for the diagonal elements $q_{ii} = (0.0001 \ v_k)^2$, with $i \in [14, 15, ..., 26]$ and v_k the acceleration input. The initial covariance matrix \mathbf{P}_0 is also a diagonal matrix with its diagonal entries equal to $p_{ij} = [(0.2\hat{x}_0^i)^2 + 0.001]$, where $j \in [1, 2, ..., n]$ and \hat{x}_0^j is the j^{th} element of the assumed initial state vector $\hat{\mathbf{x}}_0$. All initial unknown parameter values are provided in Figs. 5-8, accordingly for each example.

5.1. Example 1: Dual state-parameter estimation for nonlinear system

In this first example, acceleration measurements are available for all DOFs of the nonlinear system in Fig. 4. A notable 5% signal-to-noise ratio (SNR) is assumed, that contaminates both the acceleration input and the observed acceleration measurements at all DOFs. All the damping, stiffness parameters, and Bouc-Wen parameters are assumed to be time invariant with their exact values listed in Tables 5 and 6. Initial values of the unknown parameters are indicated in Fig. 5, presenting initial errors in the range of 30%-83%. Note that such large errors in the initial values and the significant noise levels are selected to analyze and validate the robustness of the suggested filter under these settings.

As seen in Fig. 5, both filters are performing extremely well in this case and S3F is achieving an identical performance with the UKF for all states and parameter estimates, albeit at a \sim 50% reduced computational time as compared to the UKF, due to its decreased sigma points set size. Fig. 5(a) showcases the base excitation the system is subjected to, without any added noise, Figs. 5(b-c) illustrate representative dynamic state estimations, and Figs. 5(d-h) show the online parameters identification. In all Figs. 5(b-h) exact values are also shown for comparison, along with the S3F and UKF estimates. In particular, Fig. 5(b) provides the displacement time history of the first DOF, and Fig. 5(c) displays the variation of the hysteretic deformation with respect to the displacement, again for the first DOF. Figs. 5(d-e) show the damping and stiffness identification for all DOFs, and Figs. 5(f-h) exhibit the Bouc-Wen parameters related to the nonlinear DOFs. All figures indicate that the

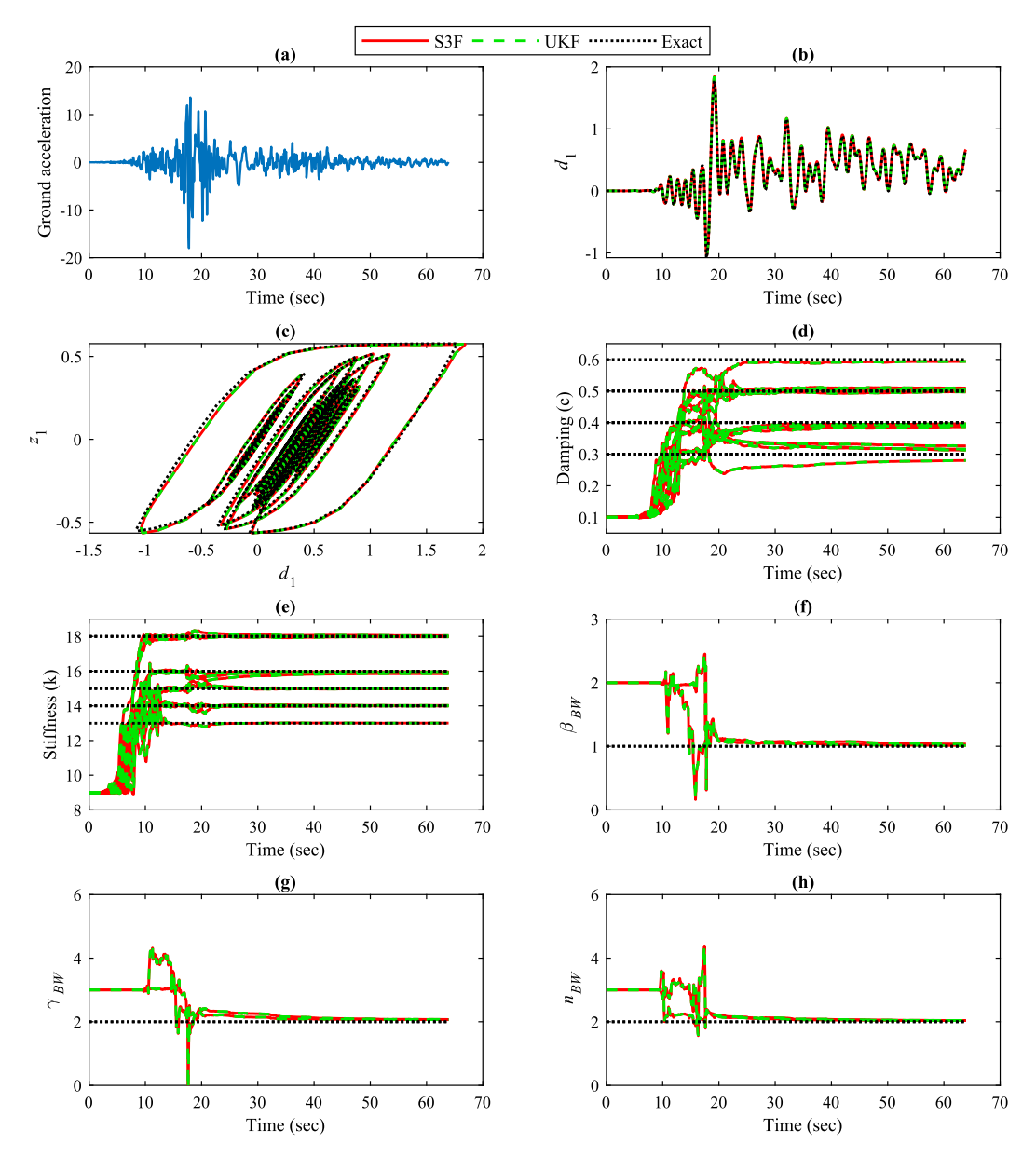


Fig. 5. Parameter and state estimation using S3F and UKF for 13-DOF nonlinear system with 5% SNR and acceleration measurements for all DOFs.

Table 5Exact damping and Bouc-Wen parameter values for the 13-DOF nonlinear system.

	Damping parameters				Bouc-Wen parameters		
Parameters	$c_1 - c_4$	$c_5 - c_8$	$c_9 - c_{12}$	c ₁₃	β_{BW}	γ_{BW}	n _{BW}
Exact values	0.3	0.4	0.5	0.6	1	2	2

dynamic states are correctly identified, and all the damping, stiffness, and Bouc-Wen parameters are converging to their respective true values largely within the first 20 s of the excitation.

5.2. Example 2: Dual estimation for nonlinear system with time-variant parameters

To further increase the complexity of the analyzed example, the stiffness parameters, which have been kept constant in the previous example, are now changing with time, as shown in Table 7, where it is indicated that the stiffness parameters

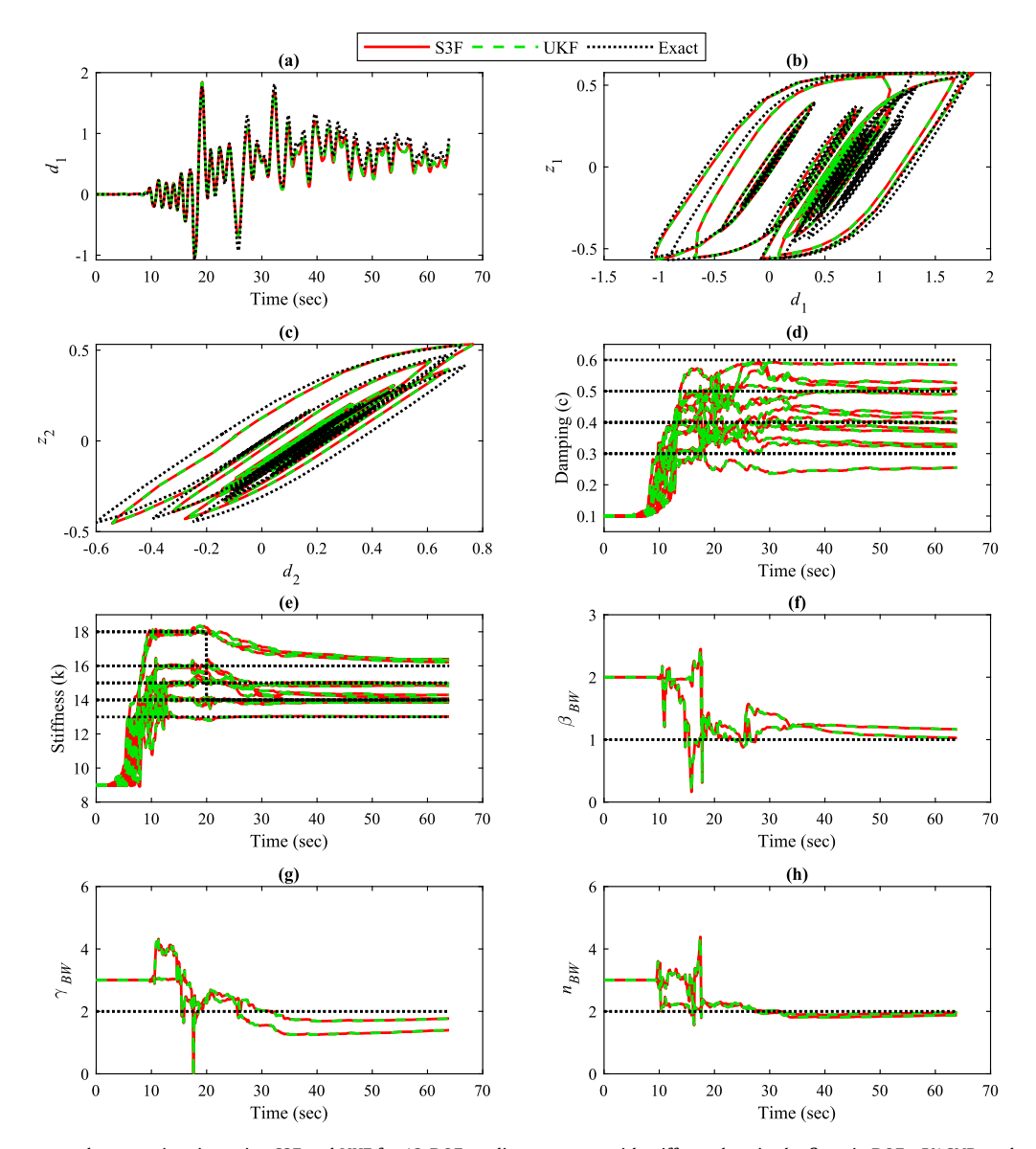


Fig. 6. Parameter and state estimation using S3F and UKF for 13-DOF nonlinear system with stiffness drop in the first six DOFs, 5% SNR, and acceleration measurements for all DOFs.

for the first six DOFs are instantaneously reduced at the 20th second of the seismic excitation. The rationale of the example is based on the assumption that the system may undergo damage and loss in stiffness which was not expected and modeled apriori with appropriate nonlinear formulations, similar to the ones used for DOFs 1 and 2. The damping and Bouc-Wen parameters still remain the same as in the previous example, and their values can be seen in Table 5, while acceleration measurements are again observed for all DOFs, and their values, as well as the ground acceleration, are contaminated with 5% SNR. Initial parameter values are also considered to be the same as in the previous example, again indicating significant errors in the initial parameter assumptions.

To simulate the target dynamic response, two different models are employed here based on different parameter values at different time instants. For the first 20 s, the responses are obtained with the zero-initial state conditions and the stiffness parameters listed in the second row of Table 7. After 20 s, the model uses the parameters of the third row, with the initial conditions given by the final state outputs of the first model. The results are presented as the exact data in Fig. 6. For the filtering process, the same model is used as in the previous example, without accounting for this stiffness change effect. Therefore, besides the complexity increase of the identification process in relation to time variant parameters, this example also studies modeling discrepancy effects, as different modeling assumptions are now made for simulation and identification.

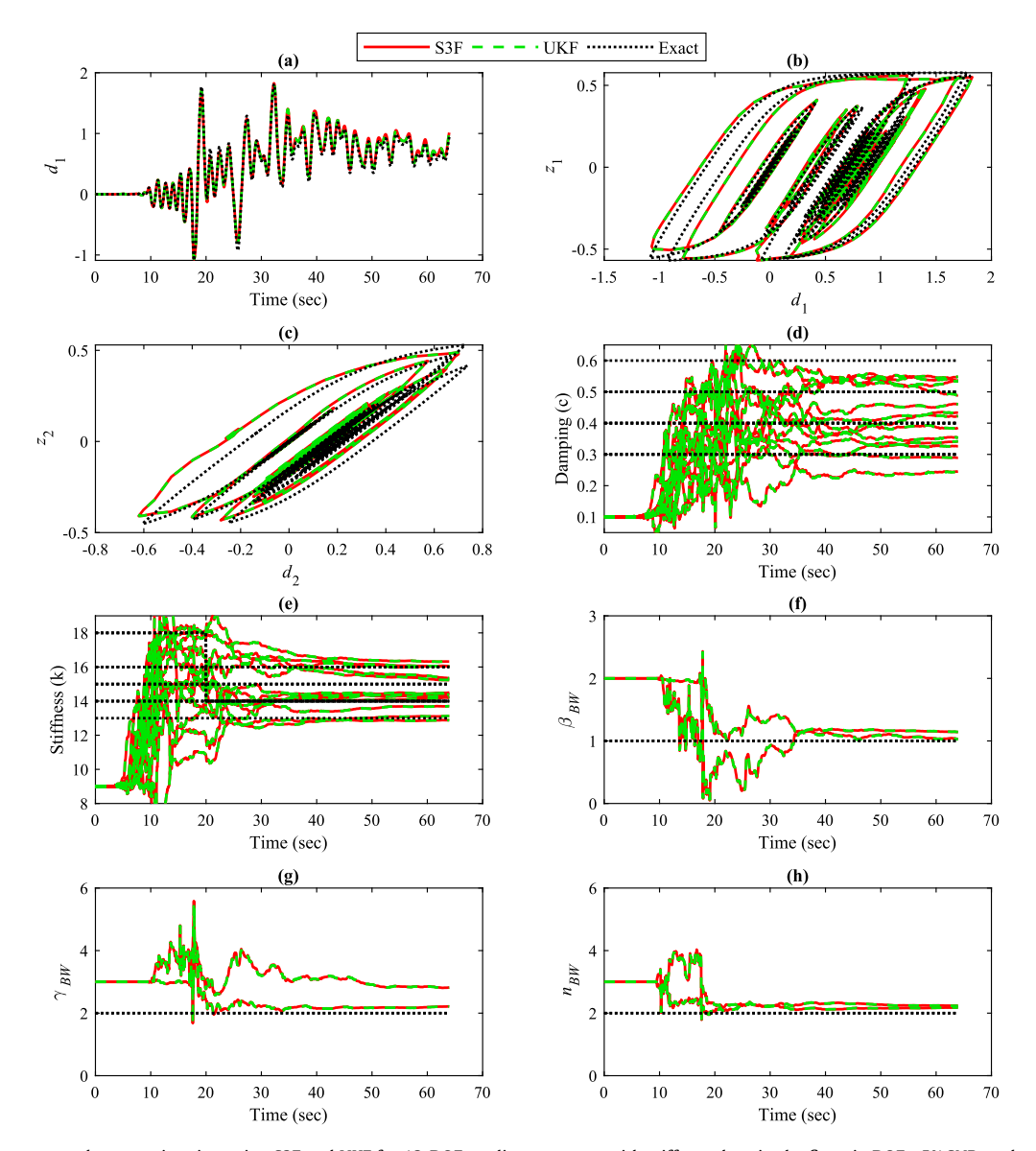


Fig. 7. Parameter and state estimation using S3F and UKF for 13-DOF nonlinear system with stiffness drop in the first six DOFs, 5% SNR, and acceleration measurements for DOFs 1–6-8–13.

Table 6Exact stiffness parameter values for 13-DOF nonlinear system for numerical examples 1 and 4.

Stiffness	k_1, k_2, k_3	k_4, k_5, k_6	k_7, k_8, k_9	k_{10}, k_{11}, k_{12}	k ₁₃
Exact values	18	16	15	14	13

Table 7 Exact stiffness parameter values for the 13-DOF nonlinear system for numerical examples 2 and 3.

Stiffness	k_1, k_2, k_3	k_4, k_5, k_6	k_7, k_8, k_9	k_{10}, k_{11}, k_{12}	k ₁₃
Exact values (0-20 sec)	18	16	15	14	13
Exact values (20 sec onwards)	16	14	15	14	13

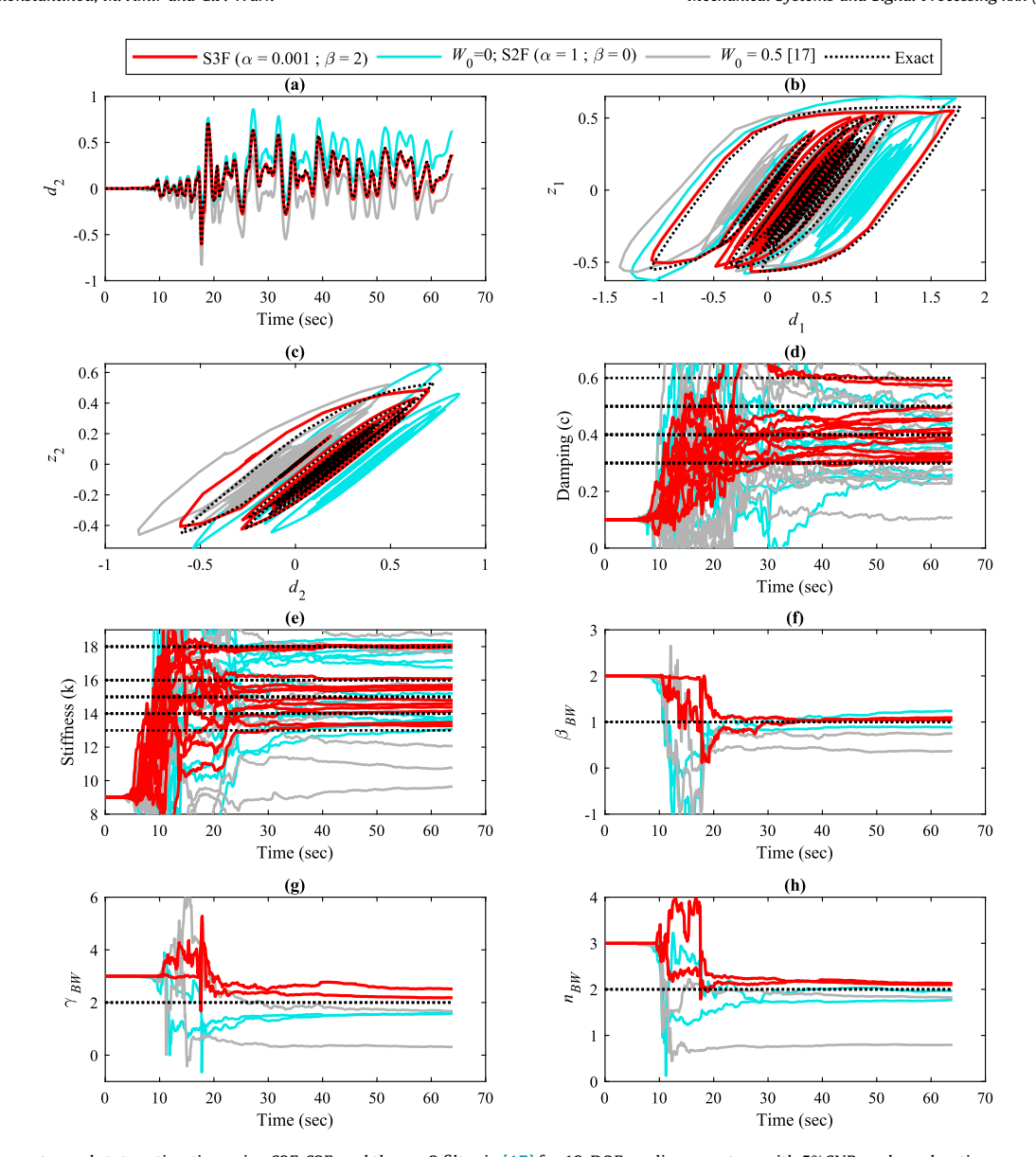


Fig. 8. Parameter and state estimation using S3F, S2F, and the n + 2 filter in [17] for 13-DOF nonlinear system with 5% SNR, and acceleration measurements for DOFs 1–6-8–13.

The UKF and S3F responses for the dynamic state estimations are shown in Figs. 6(a-c), and parameter identification results can be seen in Figs. 6(d-h). Both filters are again performing very well, however, their performance has slightly deteriorated as compared to the previous example, due to the increase in the complexity of the problem. Again, the exact same behavior is observed for both UKF and S3F at each and every time instant. In Fig. 6(e) it can be observed that in the first 20 s the filters are accurately estimating the true stiffness before the drop. After 20 s, the stiffness estimates are evolving, to again predict the new reduced stiffness of the system. As such, the time at which damage is induced can also be properly identified.

5.3. Example 3: Dual estimation with sparse measurement data and time-variant parameters

Increasing the complexity of the problem even further, now only the accelerations at the DOFs 1, 6, 8 and 13 are observed (i.e. O: 1–6-8–13), instead of all DOFs, and again 5% SNR is added for all observations and the input ground excitation. The same model as in the previous example is adopted, where the stiffness parameters are changing over time. The true parameter values can be seen in Tables 5 and 7, and the initial assumed values again remain significantly distant from the true ones, as can be also seen in Fig. 7. Due to the further increase in the complexity of the problem, some of the parameters

are not converging to the exact true values now, contrary to the previous two examples, however, they are still providing good estimates, as shown in Fig. 7, with only four measurements. Note that the displacement and hysteretic responses and filtering estimates of the second DOF are again shown in Fig. 7(c), a DOF which is however completely unobserved in this case. Many more arrangements with various combinations of four acceleration observations have also been analyzed, for example 0:1–2–8–13, 0:1–5–9–13 and so on, and they produce either similar or slightly deteriorating results, which are not shown here for brevity. The performance of the filters is further worsened for three or fewer acceleration measurements, especially for the parameter estimates. Again, these cases are not shown here for brevity.

Noteworthy in Fig. 7 is once more the similarity of the two filters for all states and parameters, which is the main scope of this paper, and same results have been also observed, as expected, for all other cases which are not reported here. Therefore, despite the high level of nonlinearity, sparsity of measurements, model discrepancies, presence of time-variant parameters, and large observation and input noise levels, the behavior of the UKF and S3F are exactly the same for both state estimates and parameter identification, as also theoretically explained earlier in this paper.

5.4. Example 4: Comparison with other filter variants

In this example, the importance of the scaling factors is examined, by comparing the S3F estimates with two other filter variants that do not consider scaling effects. The first filter is the n + 2 sigma points filter from [17], that selects the central sigma point weight W_0 for the mean and covariance estimates in the range 0–1, with W_0 = 0.5 selected here for the present illustration. The second filter, S2F, presented also earlier, requires the minimum number of sigma points, n + 1, since the central sigma point is no longer used, with weight $W_0 = 0$, as can be also obtained by substituting $\alpha = 1$ and $\beta = 0$ in the S3F. For the filtering process, accelerations at the DOFs 1, 6, 8 and 13 are assumed to be observed, and the SNR level remains the same as in the previous examples. All parameters are time-invariant in this case and their true values are listed in Tables 5 and 6. Filtering results are presented in Fig. 8. In this figure, UKF results are not shown, since they are once more found to be exactly the same as the S3F results, with α = 0.001 and β = 2, consistent with the theoretical analysis and the previous examples. As can be seen in Fig. 8, the performance of both filter variants is worse as compared to the S3F, for both states and parameters estimations. Note again here that the displacement and hysteretic responses of the second DOF are now shown in Figs. 8(a,c), a DOF which is completely unobserved in this example as well, and still the S3F estimates are able to provide a high prediction accuracy, in contrast to the other two filters. Since the identification errors in Figs. 8(d-e) are significant, for illustrative and comparative purposes the percentage errors for the damping and stiffness parameter estimates are shown in Fig. 9. As seen in the figure, while S3F error estimates are consistently converging to small values, large errors are observed in both stiffness and damping estimates for the other two filter variants, with $W_0 = 0$ and $W_0 = 0.5$, because of the higher order terms importance in nonlinear, complex problems.

In general, in the absence of any proper scaling effects, the performance of asymmetric sigma point filtering schemes significantly deteriorates, and their behavior is no longer similar to the UKF. By just including one additional, central sigma point to the S2F scheme, and proper scaling, the S3F estimates become essentially identical to the UKF ones, in all cases.

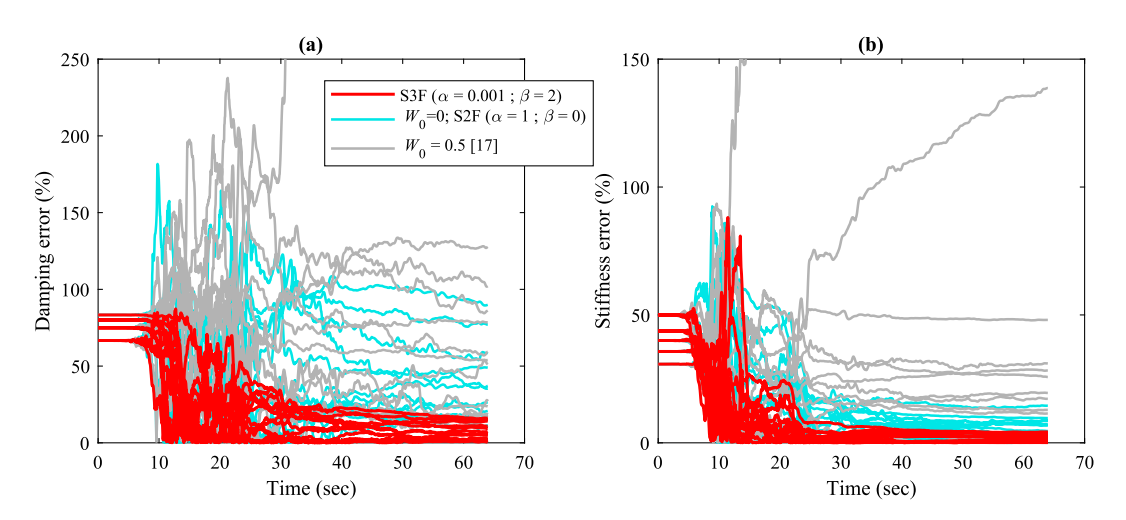


Fig. 9. Error estimates for the damping and stiffness parameters using various filters for 13-DOF nonlinear system with 5% SNR and acceleration measurements for DOFs 1–6-8–13.

5.5. Discussion of the numerical results

To illustrate the efficiency, consistency and numerical stability of the proposed S3F, four numerical examples have been presented, characterized by considerable nonlinearity, notable noise levels, time-variant and invariant parameters, significant initial parameters discrepancy from exact values, modeling errors, and sparse measurements. In all examples, the S3F achieves the same level of robustness and accuracy as the UKF, as also theoretically proven and expected, and can be implemented in exactly the same manner as the UKF. Numerous other initial values and noise levels have also been tested, and it is again observed that both filters are performing in the same manner, even with extremely high noise levels. Naturally, with the increase in the noise levels, prediction errors are similarly increasing for both UKF and S3F. For consistency and brevity, only one set of noise level and initial parameters is thus used in all examples, and generic \mathbf{R}_k , \mathbf{Q}_k , and \mathbf{P}_0 matrices are selected, since the filters' relative performance with respect to each other is not sensitive to these values. Likewise, various sparse observation settings have also been tested, and in all cases equivalent S3F and UKF accuracy is attained. In all examples, the CPU time for the S3F cases is approximately 50% reduced as compared to the UKF cases, regardless of the system configuration and the problem complexity. This computational time reduction is attributed to the pertinent reduced number of model calls, as well as the related reduction in matrix operations, since the size of all relevant matrices is almost half in S3F as compared to the UKF. Overall, S3F can be unrestrictedly utilized in all general applications where UKF can be used, while achieving in all cases an equivalent accuracy and numerical stability, albeit at a ~50% reduced computational effort.

6. Conclusions

An efficient and robust online nonlinear system identification approach, referred to as Scaled Spherical Simplex Filter (S3F), is presented in this work, that requires almost half the number of sigma points compared to the state-of-the-art UKF, while nearly achieving the exact same accuracy and numerical stability in all cases. For a general *n*-dimensional system, the *n* + 2 used sigma points, their corresponding weights, and their scaling parameters are suggested and explained in detail. The equivalence between the UKF and S3F accuracy is proven through theoretical derivations and several examples that compare the estimated mean and covariance outputs of nonlinear functions, assuming bivariate input cases described by correlated Gaussian and lognormal random variables, as well as an arbitrarily defined joint density function. Lastly, numerical examples are provided for a 13-DOF nonlinear system with varied levels of complexity, including hysteretic behavior, dual state-parameter estimation, sparsity of measurements, time-variant and invariant parameters, model error effects, and large observation and input noise levels, to showcase the capabilities and advantages of the suggested approach under very general conditions.

The performance of the S3F filter is observed to be remarkably good and robust, exhibiting identical performance to the UKF in all cases, yet requiring almost half computational demands, making it an ideal candidate for use in larger systems and online identification. The absolute minimum number of sigma points needed is achieved by eliminating the central point and scaling effects in the S3F, however, this extra point is particularly important for accuracy and suppression of errors associated with higher order terms. Overall, based on our study, we have not observed any disadvantages of the S3F in relation to the UKF, and the suggested filter can be readily utilized and similarly implemented in all relevant applications where UKF is used.

CRediT authorship contribution statement

Konstantinos G. Papakonstantinou: Conceptualization, Methodology, Software, Formal analysis, Investigation, Resources, Data curation, Writing - original draft, Writing - review & editing, Visualization, Supervision, Project administration, Funding acquisition. **Mariyam Amir:** Methodology, Software, Formal analysis, Investigation, Data curation, Writing - original draft, Writing - review & editing, Visualization. **Gordon P. Warn:** Conceptualization, Methodology, Resources, Writing - original draft, Writing - review & editing, Supervision, Project administration.

Declaration of competing interest

The authors declare that they have no known competing financial interests or personal relationships that could have appeared to influence the work reported in this paper.

Acknowledgements

This material is based upon work supported by the U.S. National Science Foundation under CAREER Grant No. 1751941.

Appendix

Higher moments and gradients for theoretical example 1

Evaluating gradients: Gradients for the Taylor series expansion, $\nabla^k f$, for $f(x) = x_1 x_2$ are obtained as:

K.G. Papakonstantinou, M. Amir and G.P. Warn

$$\begin{split} \nabla f &= \left\{ \frac{\partial f}{\partial x_1} \, \frac{\partial f}{\partial x_2} \right\} = \left\{ x_2 \, x_1 \right\} = \left\{ \mu_2 \, \mu_1 \right\} \\ \nabla^2 f &= \left\{ \frac{\partial \nabla f}{\partial x_1} \, \frac{\partial \nabla f}{\partial x_2} \right\} = \left\{ 0 \, 1 \, 1 \, 0 \right\} \\ \nabla^3 f &= \left\{ \frac{\partial \nabla^2 f}{\partial x_1} \, \frac{\partial \nabla^2 f}{\partial x_2} \right\} = \left\{ 0 \, 0 \, 0 \, 0 \, 0 \, 0 \, 0 \, 0 \right\} \end{split}$$

where μ_1 and μ_2 are the mean values for the random variables x_1 and x_2 respectively.

Evaluating Moments: Similarly, the vector $\delta \mathbf{x}^i$ can be expanded as:

$$\delta \mathbf{x} = \{ \delta x_1 \quad \delta x_2 \}^T
\delta \mathbf{x}^2 = \{ \delta x_1^2 \quad \delta x_1 \delta x_2 \quad \delta x_2 \delta x_1 \quad \delta x_2^2 \}^T
\delta \mathbf{x}^3 = \{ \delta x_1^3 \quad \delta x_1^2 \delta x_2 \quad \delta x_1^2 \delta x_2 \quad \delta x_1 \delta x_2^2 \quad \delta x_1 \delta x_2^2 \quad \delta x_1 \delta x_2^2 \quad \delta x_1^2 \delta x_2 \quad \delta x_1^2 \delta x_2^2 \quad \delta x_1^2 \delta x_1^2 \delta x_2^2 \quad \delta x_1^2 \delta$$

CASE A) Assuming Gaussian distribution (GRV)

For a multivariate Gaussian distribution of size n, $\mathbf{x} = \{x_1 x_2 \dots x_n\}^T$, with mean $\boldsymbol{\mu}_{\mathbf{x}}$ and variance $\mathbf{P}_{\mathbf{xx}}$, the moment generating function is given by:

$$M_{\mathbf{x}}(\mathbf{t}) = \exp\left(\mathbf{t}^T \mathbf{\mu}_{\mathbf{x}} + \frac{1}{2} \mathbf{t}^T \mathbf{P}_{\mathbf{x}\mathbf{x}} \mathbf{t}\right) \quad ; \quad \mathbf{t} = \left\{t_1 \ t_2 \cdots t_n\right\}^T$$

By differentiating the moment generating function with respect to \mathbf{t} , the k^{th} moment can be evaluated as:

$$E[x_1^{k_1}x_2^{k_2}\cdots x_n^{k_n}] = \frac{\partial^k M_{\mathbf{x}}(\mathbf{t})}{\partial t_1^{k_1}\partial t_2^{k_2}\cdots \partial t_n^{k_n}}\bigg|_{\mathbf{t}=\mathbf{0}} \quad \text{s.t.} \quad k = k_1 + k_2 + \cdots + k_n$$

Next, the k^{th} central moment can be obtained as:

$$E[\delta x_1^{k_1}\delta x_2^{k_2}\cdots\delta x_n^{k_n}] = E\Big[(x_1 - E[x_1])^{k_1}(x_2 - E[x_2])^{k_2}\cdots(x_n - E[x_n])^{k_n}\Big]$$

Therefore, for the given bivariate case, the moment generating function and the resulting central moments, up to 4th moment, are expressed as:

$$M_{\mathbf{x}}(\mathbf{t}) = \exp\left(t_1 \mu_1 + t_2 \mu_2 + \left(\frac{t_1 m_{11}}{2} + \frac{t_2 m_{12}}{2}\right) t_1 + \left(\frac{t_1 m_{12}}{2} + \frac{t_2 m_{22}}{2}\right) t_2\right)$$

Moment evaluations for GRV

First Moment:

$$\begin{split} E[x_1] &= \left. \mu_1 \left(= \frac{\partial M_{\mathbf{x}}(\mathbf{t})}{\partial t_1} \right|_{\mathbf{t} = \{0 \ 0\}^T} \right) \quad ; \quad E[x_2] &= \left. \mu_2 \left(= \frac{\partial M_{\mathbf{x}}(\mathbf{t})}{\partial t_2} \right|_{\mathbf{t} = \{0 \ 0\}^T} \right) \\ E[\delta x_1] &= \mathbf{0} \quad ; \quad E[\delta x_2] &= \mathbf{0} \end{split}$$

Second Moment:

$$\begin{split} E\left[x_{1}^{2}\right] &= \mu_{1}^{2} + m_{11} \left(= \frac{\partial^{2} M_{\mathbf{x}}(\mathbf{t})}{\partial t_{1}^{2}} \bigg|_{\mathbf{t} = \{0 \ 0\}^{T}} \right) \\ E\left[x_{1}x_{2}\right] &= \mu_{1}\mu_{2} + m_{12} \left(= \frac{\partial^{2} M_{\mathbf{x}}(\mathbf{t})}{\partial t_{1} \partial t_{2}} \bigg|_{\mathbf{t} = \{0 \ 0\}^{T}} \right) \\ E\left[x_{2}^{2}\right] &= \mu_{2}^{2} + m_{22} \left(= \frac{\partial^{2} M_{\mathbf{x}}(\mathbf{t})}{\partial t_{2}^{2}} \bigg|_{\mathbf{t} = \{0 \ 0\}^{T}} \right) \\ E\left[\delta x_{1}^{2}\right] &= m_{11} \quad ; \quad E\left[\delta x_{1} \delta x_{2}\right] = m_{12} \quad ; \quad E\left[\delta x_{2}^{2}\right] = m_{22} \end{split}$$

Third Moment:

$$\begin{split} E\big[x_1^3\big] &= \mu_1(\mu_1^2 + 3m_{11}) \;\; ; \;\; E\big[x_1^2x_2\big] = \mu_2(\mu_1^2 + m_{11}) + 2\mu_1m_{12} \;\; ; \;\; E\big[x_2^3\big] = \mu_2(\mu_2^2 + 3m_{22}) \\ E\big[x_1x_2^2\big] &= \mu_1(\mu_2^2 + m_{22}) + 2\mu_2m_{12} \;\; ; \;\; E\big[\delta x_1^3\big] = E\big[\delta x_1^2\delta x_2\big] = E\big[\delta x_1\delta x_2^2\big] = E\big[\delta x_2^3\big] = 0 \end{split}$$

Fourth Moment:

$$\begin{split} E\left[x_{1}^{4}\right] &= \mu_{1}^{4} + 3m_{11}^{2} + 6m_{11}\mu_{1}^{2} \\ E\left[x_{1}^{3}x_{2}\right] &= \mu_{1}^{3}\mu_{2} + 3m_{12}\mu_{1}^{2} + 3\mu_{1}m_{11}\mu_{2} + 3m_{12}m_{11} \\ E\left[x_{1}^{2}x_{2}^{2}\right] &= (\mu_{2}^{2} + m_{22})\mu_{1}^{2} + 4\mu_{1}\mu_{2}m_{12} + \mu_{2}^{2}m_{11} + 2m_{12}^{2} + m_{22}m_{11} \\ E\left[x_{1}x_{2}^{3}\right] &= \mu_{1}\mu_{2}^{3} + 3m_{12}\mu_{2}^{2} + 3\mu_{1}m_{22}\mu_{2} + 3m_{12}m_{22} \\ E\left[x_{2}^{4}\right] &= \mu_{2}^{4} + 3m_{22}^{2} + 6m_{22}\mu_{2}^{2} \\ E\left[\delta x_{1}^{4}\right] &= 3m_{11}^{2} \\ E\left[\delta x_{1}^{3}\delta x_{2}\right] &= 3m_{11}m_{22} \\ E\left[\delta x_{1}^{2}\delta x_{2}^{2}\right] &= m_{11}m_{22} + 2m_{12}^{2} \\ E\left[\delta x_{1}\delta x_{2}^{3}\right] &= 3m_{12}m_{22} \\ E\left[\delta x_{1}^{4}\delta x_{2}^{3}\right] &= 3m_{12}m_{22} \\ E\left[\delta x_{1}^{4}\delta x_{2}^{3}\right] &= 3m_{22}^{2} \end{split}$$

Exact transformed mean and variance for GRV

From the evaluated moments, the true mean and variance for *y* is given by:

$$E[y] = E[x_1x_2] = \mu_1\mu_2 + m_{12}$$

$$P_{yy} = E[y^2] - (E[y])^2 = E[x_1^2x_2^2] - (E[x_1x_2])^2 = \mu_2^2m_{11} + 2\mu_1\mu_2m_{12} + \mu_1^2m_{22} + m_{12}^2 + m_{22}m_{11}$$

Scaled Taylor estimates for GRV

Similarly, scaled Taylor approximations for the mean and covariance are obtained as:

$$\begin{split} \overline{\mathbf{f}(\mathbf{x})} &= \overline{\mathbf{y}} = \mathbf{f}(\overline{\mathbf{x}}) + \frac{1}{2} \nabla^2 \mathbf{f} E \big[\delta \mathbf{x}^2 \big] + \frac{1}{6} \nabla^3 \mathbf{f} \ \alpha E \big[\delta \mathbf{x}^3 \big] \ = \ \mu_1 \mu_2 + \ m_{12} \\ \mathbf{P}_{\mathbf{y}\mathbf{y}} &= \nabla \mathbf{f} \ \mathbf{P}_{\mathbf{x}\mathbf{x}} \nabla \mathbf{f}^T + \alpha \frac{1}{2} \Big(\nabla^2 \mathbf{f} \ E \big[\delta \mathbf{x}^2 \delta \mathbf{x}^T \big] \nabla \mathbf{f}^T + \nabla \mathbf{f} \ E \big[\delta \mathbf{x}^T \delta \mathbf{x}^2 \big] \nabla^2 \mathbf{f}^T \Big) + \\ \alpha^2 \frac{1}{4} \nabla^2 \mathbf{f} \Big(E \big[\delta \mathbf{x}^2 \delta \mathbf{x}^{2T} \big] - E \big[\delta \mathbf{x}^2 \big] E \big[\delta \mathbf{x}^2 \big]^T \Big) \nabla^2 \mathbf{f}^T + \\ \alpha^2 \frac{1}{6} \Big(\nabla^3 \mathbf{f} \ E \big[\delta \mathbf{x}^3 \delta \mathbf{x}^T \big] \nabla \mathbf{f}^T + \nabla \mathbf{f} \ E \big[\delta \mathbf{x}^T \delta \mathbf{x}^3 \big] \nabla^3 \mathbf{f}^T \Big) \\ &= m_{11} \mu_2^2 + 2\mu_1 \mu_2 m_{12} + \mu_1^2 m_{22} + \alpha^2 \Big(m_{12}^2 + m_{11} m_{22} \Big) \end{split}$$

CASE B) Assuming lognormal distribution (LN)

For a multivariate lognormal distribution of size n, $\mathbf{x} = \{x_1 x_2 \dots x_n\}^T$, with mean $\mathbf{\mu}_{\mathbf{x}}$ and variance $\mathbf{P}_{\mathbf{x}\mathbf{x}}$, higher order moments can be easily evaluated from the moment generating function of the normal distribution.

Assume z is given by $z = \log(x)$. Therefore, z is a GRV with mean μ_z and variance P_{zz} . Using the previous definition, the moment generating function of z is given by:

$$M_{\mathbf{z}}(\mathbf{t}) = \exp\left(\mathbf{t}^{T} \boldsymbol{\mu}_{\mathbf{z}} + \frac{1}{2} \mathbf{t}^{T} \mathbf{P}_{\mathbf{z}\mathbf{z}} \mathbf{t}\right) \quad ; \quad \mathbf{t} = \left\{t_{1} \ t_{2} \cdots t_{n}\right\}^{T}$$
where, $\mu_{zi} = \log(\mu_{i}) - \frac{1}{2} \log\left(\frac{m_{ii}}{\mu_{i}^{2}} + 1\right) \; ; \quad m_{zij} = \log\left(\frac{m_{ij}}{\mu_{i} \mu_{j}} + 1\right) \; ; \quad \text{s.t.} \quad i, j \in \{1, 2, \dots, n\}$

 μ_{zi} is the i^{th} element of vector $\boldsymbol{\mu_z}$, and m_{zij} is the element of matrix $\boldsymbol{P_{zz}}$ in the i^{th} row and j^{th} column, whereas μ_i is the i^{th} element of vector $\boldsymbol{\mu_x}$, and m_{ii} is the element of matrix $\boldsymbol{P_{xx}}$ in the i^{th} row and j^{th} column.

The k^{th} moment can be evaluated as:

$$E[x_1^{k_1}x_2^{k_2}\cdots x_n^{k_n}] = E[e^{k_1z_1+k_2z_2+\cdots+k_nz_n}] = M_{\mathbf{z}}(\mathbf{t})|_{\mathbf{t}=\{k_1\ k_2\ \cdots\ k_n\}^T} \quad \text{s.t.} \quad k = k_1 + k_2 + \cdots + k_n$$

$$E[\delta x_1^{k_1}\delta x_2^{k_2}\cdots \delta x_n^{k_n}] = E\Big[(x_1 - E[x_1])^{k_1}(x_2 - E[x_2])^{k_2}\cdots (x_n - E[x_n])^{k_n}\Big]$$

Therefore, for the given bivariate case, the moment generating function and the resulting central moments, up to 4th moment, are expressed as:

K.G. Papakonstantinou, M. Amir and G.P. Warn

GRV:
$$\mathbf{z} = \log(\mathbf{x})$$
; $\mathbf{z} = \begin{Bmatrix} z_1 \\ z_2 \end{Bmatrix} = \begin{Bmatrix} \log x_1 \\ \log x_2 \end{Bmatrix}$; $\boldsymbol{\mu}_{\mathbf{z}} = E[\mathbf{z}] = \begin{Bmatrix} \mu_{z1} \\ \mu_{z2} \end{Bmatrix}$; $\mathbf{P}_{\mathbf{z}\mathbf{z}} = \begin{bmatrix} m_{z11} & m_{z12} \\ m_{z12} & m_{z22} \end{bmatrix}$
 $M_{\mathbf{z}}(\mathbf{t}) = E[e^{\mathbf{t}^T\mathbf{z}}] = \exp\left(t_1\mu_{z1} + t_2\mu_{z2} + \left(\frac{t_1m_{z11}}{2} + \frac{t_2m_{z12}}{2}\right)t_1 + \left(\frac{t_1m_{z12}}{2} + \frac{t_2m_{z22}}{2}\right)t_2\right)$

Moment evaluations for LN

First Moment:

$$\begin{array}{l} \textit{E}[\textit{x}_1] = \; \mu_1 \; \left(= \; \textit{M}_{\textbf{z}}(\textbf{t}) |_{\, \textbf{t} = \{1 \quad 0\}^T} \right) \quad ; \; \textit{E}[\textit{x}_2] = \; \mu_2 \; \left(= \; \textit{M}_{\textbf{z}}(\textbf{t}) |_{\, \textbf{t} = \{0 \quad 1\}^T} \right) \\ \textit{E}[\delta \textit{x}_1] = \; 0 \quad ; \; \textit{E}[\delta \textit{x}_2] = \; 0 \end{array}$$

Second Moment:

$$\begin{split} E\left[x_{1}^{2}\right] &= \mu_{1}^{2} + m_{11} \left(= M_{\mathbf{z}}(\mathbf{t})|_{\mathbf{t} = \{2 \ 0\}^{T}}\right) \\ E\left[x_{1}x_{2}\right] &= \mu_{1}\mu_{2} + m_{12} \left(= M_{\mathbf{z}}(\mathbf{t})|_{\mathbf{t} = \{1 \ 1\}^{T}}\right) \\ E\left[x_{2}^{2}\right] &= \mu_{2}^{2} + m_{22} \left(= M_{\mathbf{z}}(\mathbf{t})|_{\mathbf{t} = \{0 \ 2\}^{T}}\right) \\ E\left[\delta x_{1}^{2}\right] &= m_{11} ; E\left[\delta x_{1}\delta x_{2}\right] &= m_{12} ; E\left[\delta x_{2}^{2}\right] &= m_{22} \end{split}$$

Third Moment:

$$\begin{split} E\left[\chi_{1}^{3}\right] &= \frac{\left(\mu_{1}^{2} + m_{11}\right)^{3}}{\mu_{1}^{3}} \; ; \; E\left[\chi_{1}^{2}\chi_{2}\right] = \frac{\left(\mu_{1}^{2} + m_{11}\right)\left(\mu_{1}\mu_{2} + m_{12}\right)^{2}}{\mu_{1}^{2}\mu_{2}} \; ; \; E\left[\chi_{1}\chi_{2}^{2}\right] \; = \frac{\left(\mu_{2}^{2} + m_{22}\right)\left(\mu_{1}\mu_{2} + m_{12}\right)^{2}}{\mu_{2}^{2}\mu_{1}} \; ; \; E\left[\chi_{2}^{3}\right] = \frac{\left(\mu_{2}^{2} + m_{22}\right)^{3}}{\mu_{2}^{3}} \\ E\left[\delta\chi_{1}^{3}\right] &= \frac{m_{11}^{2}\left(3\mu_{1}^{2} + m_{11}\right)}{\mu_{2}^{3}} \; ; \; E\left[\delta\chi_{1}^{2}\delta\chi_{2}\right] = \frac{m_{12}^{2}}{\mu_{2}} + \frac{2m_{11}m_{12}}{\mu_{1}} + \frac{m_{11}m_{12}^{2}}{\mu_{1}^{2}\mu_{2}} \; ; \; E\left[\delta\chi_{1}\delta\chi_{2}^{2}\right] = \frac{m_{22}^{2}\left(3\mu_{2}^{2} + m_{22}\right)}{\mu_{2}^{3}} \end{split}$$

Fourth Moment:

$$\begin{split} E\left[x_{1}^{4}\right] &= \frac{\left(\mu_{1}^{2} + m_{11}\right)^{6}}{\mu_{1}^{8}} \; ; \; E\left[x_{2}^{4}\right] = \frac{\left(\mu_{2}^{2} + m_{22}\right)^{6}}{\mu_{2}^{8}} \; ; E\left[x_{1}^{3}x_{2}\right] = \frac{\left(\mu_{1}^{2} + m_{11}\right)^{3} \left(\mu_{1}\mu_{2} + m_{12}\right)^{3}}{\mu_{1}^{6}\mu_{2}^{2}} \\ E\left[x_{1}x_{2}^{2}\right] &= \frac{\left(\mu_{2}^{2} + m_{22}\right)^{3} \left(\mu_{1}\mu_{2} + m_{12}\right)^{3}}{\mu_{2}^{6}\mu_{1}^{2}} \; ; \; E\left[x_{1}^{2}x_{2}^{2}\right] = \frac{\left(\mu_{1}^{2} + m_{11}\right) \left(\mu_{2}^{2} + m_{22}\right) \left(\mu_{1}\mu_{2} + m_{12}\right)^{4}}{\mu_{1}^{4}\mu_{2}^{4}} \\ E\left[\delta x_{1}^{4}\right] &= 3m_{11}^{2} + \frac{16m_{11}^{3}}{\mu_{1}^{2}} + \frac{15m_{11}^{4}}{\mu_{1}^{4}} + \frac{6m_{11}^{5}}{\mu_{1}^{6}} + \frac{m_{11}^{6}}{\mu_{1}^{8}} \; ; \; E\left[\delta x_{2}^{4}\right] = 3m_{22}^{2} + \frac{16m_{22}^{3}}{\mu_{2}^{2}} + \frac{15m_{22}^{4}}{\mu_{2}^{4}} + \frac{6m_{22}^{5}}{\mu_{2}^{5}} + \frac{m_{11}^{5}}{\mu_{1}^{8}} \; ; \; E\left[\delta x_{1}^{3}\delta x_{2}\right] = 3m_{12}m_{11} + \frac{m_{12}^{3}}{\mu_{1}^{2}} + \frac{6m_{12}^{2}m_{11}}{\mu_{1}\mu_{12}} + \frac{9m_{11}^{2}m_{12}}{\mu_{1}^{2}} + \frac{3m_{12}^{2}m_{11}}{\mu_{1}^{3}\mu_{2}} + \frac{3m_{12}^{2}m_{11}}{\mu_{1}^{4}\mu_{2}} + \frac{3m_{12}^{2}m_{12}}{\mu_{1}^{2}\mu_{2}} + \frac{3m_{12}^{2}m_{22}}{\mu_{1}^{2}\mu_{1}} + \frac{3m_{12}^{2}m_{22}}{\mu_{1}^{2}\mu_{1}^{2}} + \frac{3m_{12}^{2}m_{22}}{\mu_{1}^{2}\mu_{1}^{2}} + \frac{3m_{12}^{2}m_{22}}{\mu_{1}^{2}\mu_{1}^{2}}$$

Exact transformed mean and variance for LN

Based on the evaluated moments, the true values for the transformed mean and variance are obtained as:

$$\begin{split} E[y] &= E[x_1x_2] = \mu_1\mu_2 + m_{12} \\ P_{yy} &= E\left[y^2\right] - (E[y])^2 = E\left[x_1^2x_2^2\right] - (E[x_1x_2])^2 \\ &= \frac{\left(\mu_1^2 + m_{11}\right)\left(\mu_2^2 + m_{22}\right)\left(\mu_1\mu_2 + m_{12}\right)^4}{\mu_1^4\mu_2^4} - \left(\mu_1\mu_2 + m_{12}\right)^2 \\ &= \mu_2^2 m_{11} + 2\mu_1\mu_2 m_{12} + \mu_1^2 m_{22} + m_{11}m_{22} + 5m_{12}^2 + \frac{4\mu_1 m_{12} m_{22}}{\mu_2} + \frac{4\mu_2 m_{11} m_{12}}{\mu_1} + \frac{4m_{11} m_{12} m_{22}}{\mu_1 \mu_2} + \frac{4m_{12}^3 m_{22}}{\mu_$$

Scaled Taylor estimates for GRV

Results from the scaled Taylor approximations:

$$\begin{split} \overline{\mathbf{f}(\mathbf{x})} &= \overline{\mathbf{y}} = \mathbf{f}(\overline{\mathbf{x}}) + \frac{1}{2} \nabla^2 \mathbf{f} E \big[\delta \mathbf{x}^2 \big] + \frac{1}{6} \nabla^3 \mathbf{f} \ \alpha E \big[\delta \mathbf{x}^3 \big] \\ &= \mu_1 \mu_2 + \ m_{12} \\ \\ \mathbf{P_{yy}} &= \nabla \mathbf{f} \ \mathbf{P_{xx}} \nabla \mathbf{f}^T + \alpha \frac{1}{2} \left(\nabla^2 \mathbf{f} \ E \big[\delta \mathbf{x}^2 \delta \mathbf{x}^T \big] \nabla \mathbf{f}^T + \nabla \mathbf{f} \ E \big[\delta \mathbf{x}^T \delta \mathbf{x}^2 \big] \nabla^2 \mathbf{f}^T \right) \\ &+ \alpha^2 \frac{1}{4} \nabla^2 \mathbf{f} \left(E \big[\delta \mathbf{x}^2 \delta \mathbf{x}^{2T} \big] - E \big[\delta \mathbf{x}^2 \big] E \big[\delta \mathbf{x}^2 \big]^T \right) \nabla^2 \mathbf{f}^T \\ &+ \alpha^2 \frac{1}{6} \left(\nabla^3 \mathbf{f} \ E \big[\delta \mathbf{x}^3 \delta \mathbf{x}^T \big] \nabla \mathbf{f}^T + \nabla \mathbf{f} \ E \big[\delta \mathbf{x}^T \delta \mathbf{x}^3 \big] \nabla^3 \mathbf{f}^T \right) \\ &= m_{11} \mu_2^2 + 2 \mu_1 \mu_2 m_{12} + \mu_1^2 m_{22} + \alpha \left(\frac{4 \mu_1 m_{12} m_{22}}{\mu_2} + 4 m_{12}^2 + \frac{4 \mu_2 m_{11} m_{12}}{\mu_1} + \frac{2 m_{12}^2 m_{22}}{\mu_2^2} + \frac{2 m_{12}^2 m_{11}}{\mu_1^2} \right) \\ &+ \alpha^2 \left(\frac{m_{11} m_{22} + m_{12}^2 + \frac{4 m_{12}^2 m_{22}}{\mu_1^2} + \frac{4 m_{11} m_{12} m_{22}}{\mu_1 \mu_2} + \frac{4 m_{12}^2 m_{12}}{\mu_1 \mu_2} + \frac{4 m_{12}^2 m_{22}}{\mu_1 \mu_2^2} + \frac{4 m_{11}^2 m_{22}}{\mu_1 \mu_2^2} + \frac{4 m_{11}^2 m_{22}}{\mu_1 \mu_2^2} + \frac{4 m_{11}^2 m_{22}}{\mu_1^2 \mu_2^2} + \frac{4 m_{12}^2 m$$

Note that when $\alpha = 1$, the true variance is exactly the same with the one from the Taylor approximation, since the higher moment terms in the Taylor expansion are all zero, except for the ones employed in the above equation.

UKF case

The weights for the Unscented Transformations are obtained as:

$$W_0^{(m)} = 1 - \frac{1}{\alpha^2} \; ; \; W_0^{(c)} = 1 - \frac{1}{\alpha^2} + (1 - \alpha^2 + \beta)$$

 $W_i^{(m)} = W_i^{(c)} = \frac{1}{4\alpha^2} \qquad i = 1, ..., 4$

The estimated mean and variance using transformed sigma points, Y_i, are given as:

$$\begin{split} E[y] &= W_0^{(m)} Y_0 + \sum_{i=1}^4 W_i^{(m)} Y_i = \mu_1 \mu_2 + m_{12} \\ P_{yy} &= W_0^{(c)} (Y_0 - E[y])^2 + \sum_{i=1}^4 W_i^{(c)} (Y_i - E[y])^2 \\ &= \mu_1 \mu_2 + m_{12} m_{11} \mu_2^2 + 2\mu_1 \mu_2 m_{12} + \mu_1^2 m_{22} + (\alpha^2 + \beta) m_{12}^2 \end{split}$$

S2F case

The weights of the sigma points are:

$$W_i = \frac{1}{2}$$
 $i = 1, ..., 3$

The estimated mean and variance using transformed sigma points, Yi, are given as:

$$\begin{split} E[y] &= \sum_{i=1}^{3} W_{i} Y_{i} = \mu_{1} \mu_{2} + m_{12} \\ P_{yy} &= \sum_{i=1}^{3} W_{i} (Y_{i} - E[y])^{2} \\ &= m_{11} \mu_{2}^{2} + 2\mu_{1} \mu_{2} m_{12} + \mu_{1}^{2} m_{22} + \frac{1}{2} m_{11} m_{22} - \sqrt{\frac{2(m_{11} m_{22} - m_{12}^{2})}{m_{11}}} (m_{11} \mu_{2} + m_{12} \mu_{1}) \end{split}$$

S3F case

The weights of the sigma points are obtained as:

K.G. Papakonstantinou, M. Amir and G.P. Warn

$$W_0^{(m)} = 1 - \frac{1}{\alpha^2}$$
 , $W_0^{(c)} = 1 - \frac{1}{\alpha^2} + (1 - \alpha^2 + \beta)$ $W_i^{(m)} = W_i^{(c)} = \frac{1}{3\alpha^2}$ $i = 1, ..., 3$

The estimated mean and variance using transformed sigma points, Y_i, are given as:

$$\begin{split} E[y] &= W_0^{(m)} Y_0 + \sum_{i=1}^3 W_i^{(m)} Y_i &= \mu_1 \mu_2 + m_{12} \\ P_{yy} &= W_0^{(c)} (Y_0 - E[y])^2 + \sum_{i=1}^3 W_i^{(c)} (Y_i - E[y])^2 \\ &= m_{11} \mu_2^2 + 2\mu_1 \mu_2 m_{12} + \mu_1^2 m_{22} + \beta m_{12}^2 + \frac{1}{2} \alpha^2 m_{11} m_{22} - \sqrt{\frac{2(m_{11} m_{22} - m_{12}^2)}{m_{11}}} \alpha (m_{11} \mu_2 + m_{12} \mu_1) \end{split}$$

Higher moments for theoretical example 2

The first four centralized moments for the Taylor series approximation are evaluated as:

First Moment
$$(l+m=1)$$
:
$$E[\delta x_1] = 0 \; ; \; E[\delta x_2] = 0$$
 Second Moment $(l+m=2)$:
$$E[\delta x_1^2] = \frac{139\pi^2}{11,520} = 0.1191 \; ; \; E[\delta x_1\delta x_2] = -\frac{\pi}{576} = -0.0055 \; ; \; E[\delta x_2^2] = \frac{11}{144} = 0.0764$$
 Third Moment $(l+m=3)$:
$$E[\delta x_1^3] = -\frac{55\pi^3}{55,296} = -0.0308 \; ; \; E[\delta x_1^2\delta x_2] = \frac{13\pi^2}{69,120} = 0.0019$$

$$E[\delta x_1\delta x_2^2] = \frac{\pi}{3,456} = 0.0009 \; ; \; E[\delta x_2^3] = -\frac{31}{4,320} = -0.0072$$
 Fourth Moment $(l+m=4)$:
$$E[\delta x_1^4] = \frac{25,021\pi^4}{61,931,520} = 0.0394 \; ; \; E[\delta x_1^3\delta x_2] = -\frac{149\pi^3}{2,211,840} = -0.0021$$

$$E[\delta x_1^2\delta x_2^2] = \frac{1,477\pi^2}{1,658,880} = 0.0088 \; ; \; E[\delta x_1\delta x_2^3] = -\frac{41\pi}{138,240} = -0.00093 \; ; \; E[\delta x_2^4] = \frac{403}{34,560} = 0.0117$$

where l + m is the order of the moment, as already defined in Eq. (32).

System matrices for numerical examples

System matrices for all numerical examples are defined as follows:

$$\mathbf{M} = \begin{bmatrix} m_1 & 0 & \cdots & 0 \\ 0 & m_2 & \cdots & 0 \\ \vdots & \vdots & \ddots & 0 \\ 0 & 0 & 0 & m_{13} \end{bmatrix}, \mathbf{C} = \begin{bmatrix} c_1 + c_2 & -c_2 & \cdots & 0 & 0 \\ -c_2 & c_2 + c_3 & \cdots & 0 & 0 \\ \vdots & \vdots & \ddots & -c_{12} & 0 \\ 0 & 0 & -c_{12} & c_{12} + c_{13} & -c_{13} \\ 0 & 0 & 0 & -c_{13} & c_{13} \end{bmatrix}$$

$$\mathbf{K} = \begin{bmatrix} k_1^e + k_2^e & -k_2^e & \cdots & 0 & 0 \\ -k_2^e & k_2^e + k_3^e & \cdots & 0 & 0 \\ \vdots & \vdots & \ddots & -k_{12}^e & 0 \\ 0 & 0 & -k_{12}^e & k_{12}^e + k_{13}^e & -k_{13}^e \\ 0 & 0 & 0 & -k_{13}^e & k_{13}^e \end{bmatrix}, \mathbf{H} = \begin{bmatrix} k_1^h & -k_2^h & 0 & \cdots & 0 & 0 \\ 0 & k_2^h & -k_3^h & \cdots & 0 & 0 \\ \vdots & \vdots & k_3^h & \cdots & 0 & 0 \\ \vdots & \vdots & \vdots & \ddots & 0 & 0 \\ 0 & 0 & 0 & 0 & k_{12}^h & -k_{13}^h \\ 0 & 0 & 0 & 0 & 0 & k_{13}^h \end{bmatrix}$$

$$k_i^e = \alpha_i k_i, \text{ and } k_i^h = (1 - \alpha_i) k_i \text{ for } i = [1, 2, \dots, 13]$$

where m_i , c_i , k_i are the mass, damping, and elastic stiffness parameters, and α_i is the post-elastic to elastic stiffness ratio for the i^{th} DOF, defined as $\alpha_i = 0$ for i=[1,2] and 1 otherwise, in all examples.

References

- [1] G. Kerschen, K. Worden, A.F. Vakakis, J.C. Golinval, Past, present and future of nonlinear system identification in structural dynamics, Mech. Syst. Sig. Process. 20 (3) (2006) 505–592.
- [2] D. Simon, Optimal State Estimation: Kalman, H infinity and Nonlinear Approaches, Wiley, New York, USA, 2006.
- [3] C.R. Farrar, K. Worden, Structural Health Monitoring: A Machine Learning Perspective, Chichester, Wiley, UK, 2012.
- [4] J.P. Noël, G. Kerschen, Nonlinear system identification in structural dynamics: 10 more years of progress, Mech. Syst. Sig. Process. 83 (2017) 2-35.
- [5] R.E. Kalman, A new approach to linear filtering and prediction problems, J. Basic. Eng-T. ASME 82 (1) (1960).
- [6] C.-B. Yun, M. Shinozuka, Identification of non-linear structural dynamic systems, J. Struct. Mech. 8 (2) (1980).
- [7] S.J. Julier, J.K. Uhlmann, Unscented filtering and nonlinear estimation, Proceedings of the IEEE 92 (3) (2004) 2004.
- [8] N.J. Gordon, D.J. Salmond, A.F. Smith, Novel approach to nonlinear/non-Gaussian Bayesian state estimation, IEE proceedings F (radar and signal processing) 140 (2) (1993) 107–113.
- [9] E.N. Chatzi, A.W. Smyth, The unscented Kalman filter and particle filter methods for nonlinear structural system identification with non-collocated heterogeneous sensing, Struct. Control Hlth. 16 (1) (2009).
- [10] S. J. Julier, J. K. Uhlmann and H. F. Durrant-Whyte, A new approach for filtering nonlinear systems, in: Proceedings of the 1995 American Control Conference, IEEE, 1995.
- [11] S.J. Julier, J.K. Uhlmann, A general method for approximating nonlinear transformations of probability distributions, Robotics Research Group, Department of Engineering Science, University of Oxford, 1996.
- [12] S. J. Julier and J. K. Uhlmann, New extension of the Kalman filter to nonlinear systems, in: Signal Processing, Sensor Fusion, and Target Recognition VI, vol. 3068, pp. 182-193. International Society for Optics and Photonics, 1997.
- [13] S. J. Julier, Skewed approach to filtering, in: Aerospace/Defense Sensing and Controls, International Society for Optics and Photonics, 1998.
- [14] N. Adurthi, P. Singla, T. Singh, Conjugate unscented transformation: Applications to estimation and control, J. Dyn. Syst. Meas. Contr. 140 (3) (2018) 030907.
- [15] D. Tenne, T. Singh, The higher order unscented filter, Proceedings of the 2003 American Control Conference, IEEE, 2003.
- [16] S.J. Julier, J.K. Uhlmann, Reduced sigma point filters for the propagation of means and covariances through nonlinear transformations, Proceedings of the 2002 American Control Conference, 2002.
- [17] S.J. Julier, The spherical simplex unscented transformation, Proceedings of the 2003 American Control Conference, 2003.
- [18] S.J. Julier, The scaled unscented transformation, Proceedings of the 2002 American Control Conference, 2002.
- [19] E. Wan and R. van der Merwe, The Unscented Kalman Filter for nonlinear estimation, in: Adaptive Systems for Signal Processing, Communications, and Control Symposium, IEEE, 2000.
- [20] R. van der Merwe, Sigma-point Kalman filters for probabilistic inference in dynamic state-space models, Doctoral dissertation, OGI School of Science & Engineering at OHSU, 2004.
- [21] S. Mariani, A. Ghisi, Unscented Kalman filtering for nonlinear structural dynamics, Nonlinear Dyn. 49 (1-2) (2007) 131-150.
- [22] M. Wu, A.W. Smyth, Real-time parameter estimation for degrading and pinching hysteretic models, Int. J. Nonlin. Mech. 43 (9) (2008).
- [23] Y. Chen, M.Q. Feng, Structural health monitoring by recursive Bayesian filtering, J. Eng. Mech. 135 (4) (2009) 231-242.
- [24] E.N. Chatzi, A.W. Smyth, S.F. Masri, Experimental application of on-line parametric identification for nonlinear hysteretic systems with model uncertainty, Struct. Saf. 32 (5) (2010) 326–337.
- [25] S.E. Azam, A. Ghisi, S. Mariani, Parallelized sigma-point Kalman filtering for structural dynamics, Comput. Struct. 92 (2012) 193-205.
- [26] R. Omrani, R.E. Hudson, E. Taciroglu, Parametric identification of nondegrading hysteresis in a laterally and torsionally coupled building using an Unscented Kalman Filter, J. Eng. Mech. 139 (4) (2012).
- [27] Z. Xie, J. Feng, Real-time nonlinear structural system identification via iterated unscented Kalman filter, Mech. Syst. Sig. Process. 28 (2012) 309–322.
- [28] W. Song, S. Dyke, Real-time dynamic model updating of a hysteretic structural system, J. Struct. Eng. 140 (3) (2013).
- [29] K.G. Papakonstantinou, M. Shinozuka, Spatial stochastic direct and inverse analysis for the extent of damage in deteriorated RC structures, Comput. Struct. 128 (2013) 286–296.
- [30] R. Schenkendorf, M. Mangold, Online model selection approach based on Unscented Kalman Filtering, J. Process Control 23 (1) (2013) 44-57.
- [31] E. Asgarieh, B. Moaveni, A. Nozari, A. R. Barbosa and E. Chatzi, Nonlinear identification of a seven-story shear wall building based on numerically simulated seismic data, in: Dynamics of Civil Structures, Volume 4 (pp. 245-254), Springer, 2014.
- [32] A. Al-Hussein, A. Haldar, Novel unscented Kalman filter for health assessment of structural systems with unknown input, J. Eng. Mech. 141 (7) (2015) 04015012.
- [33] T. Kontoroupi, A.W. Smyth, Online noise identification for joint state and parameter estimation of nonlinear systems, ASCE-ASME Journal of Risk and Uncertainty in Engineering Systems, Part A: Civil Engineering 2 (3) (2016) B4015006.
- [34] M.N. Chatzis, E.N. Chatzi, A discontinuous unscented Kalman filter for non-smooth dynamic problems, Frontiers in Built Environment 3 (2017) 56.
- [35] M.N. Chatzis, E.N. Chatzi, A.W. Smyth, On the observability and identifiability of nonlinear structural and mechanical systems, Struct. Control Hith. 22 (3) (2015) 574–593.
- [36] R. Astroza, H. Ebrahimian, J.P. Conte, Material parameter identification in distributed plasticity FE models of frame-type structures using nonlinear stochastic filtering, J. Eng. Mech. 141 (5) (2015) 04014149.
- [37] R. Astroza, H. Ebrahimian, Y. Li, J.P. Conte, Bayesian nonlinear structural FE model and seismic input identification for damage assessment of civil structures, Mech. Syst. Sig. Process. 93 (2017) 661–687.
- [38] K. Erazo, E.M. Hernandez, Bayesian model–data fusion for mechanistic postearthquake damage assessment of building structures, J. Eng. Mech. 142 (9) (2016).
- [39] A. Olivier, A.W. Smyth, On the performance of online parameter estimation algorithms in systems with various identifiability properties, Frontiers in Built Environment 3 (2017) 14.
- [40] A. Olivier, A.W. Smyth, Review of nonlinear filtering for SHM with an exploration of novel higher-order Kalman Filtering algorithms for uncertainty quantification, J. Eng. Mech. 143 (11) (2017) 04017128.
- [41] G. Yan, H. Sun, O. Buyukozturk, Impact load identification for composite structures using Bayesian regularization and unscented Kalman filter, Struct. Control Hlth. 24 (5) (2017) 1910.
- [42] W. Song, Generalized minimum variance unbiased joint input-state estimation and its unscented scheme for dynamic systems with direct feedthrough, Mech. Syst. Sig. Process. 99 (2018) 886–920.
- [43] A. Calabrese, S. Strano, M. Terzo, Adaptive constrained unscented Kalman filtering for real-time nonlinear structural system identification, Struct. Control Hlth. 25 (2) (2018) e2084.
- [44] V.K. Dertimanis, E.N. Chatzi, S.E. Azam, C. Papadimitriou, Input-state-parameter estimation of structural systems from limited output information, Mech. Syst. Sig. Process. 126 (2019) 711–746.
- [45] Y. Lei, D. Xia, K. Erazo, S. Nagarajaiah, A novel unscented Kalman filter for recursive state-input-system identification of nonlinear systems, Syst. Sig. Process. 127 (2019) 120–135.
- [46] M. Song, R. Astroza, H. Ebrahimian, B. Moaveni, C. Papadimitriou, Adaptive Kalman filters for nonlinear finite element model updating, Mech. Syst. Sig. Process. 143 (2020) 106837.
- [47] M. Amir, K.G. Papakonstantinou, G.P. Warn, A consistent Timoshenko hysteretic beam finite element model, Int. J. Nonlin. Mech. 119 (2020) 103218, https://www.sciencedirect.com/science/article/abs/pii/S0020746219300836.

ARTICLE IN PRESS

K.G. Papakonstantinou, M. Amir and G.P. Warn

Mechanical Systems and Signal Processing xxx (xxxx) xxx

- [48] M. Amir, K.G. Papakonstantinou, G.P. Warn, Hysteretic beam finite-element model including multiaxial yield/capacity surface evolution with degradations, J. Eng. Mech. 146 (9) (2020) 04020105.
- [49] M. Amir, K. G. Papakonstantinou and G. P. Warn, State-space formulation for structural analysis with coupled degradation-plasticity and geometric nonlinearity, Under Review.
- [50] M. Amir, K.G. Papakonstantinou and G. P. Warn, Scaled Spherical Simplex Filter and state-space damage-plasticity finite-element model for computationally efficient system identification, J. Eng. Mech., In Print. https://ascelibrary.org/doi/pdf/10.1061/%28ASCE%29EM.1943-7889.0001945.
- [51] K.G. Papakonstantinou, M. Shinozuka, Optimum inspection and maintenance policies for corroded structures using partially observable Markov decision processes and stochastic, physically based models, Probab. Eng. Mech. 37 (2014) 93–108.
- [52] C.P. Andriotis, K.G. Papakonstantinou, Managing engineering systems with large state and action spaces through deep reinforcement learning, Reliab. Eng. Syst. Saf. 191 (2019) 106483.
- [53] C. P. Andriotis, K. G. Papakonstantinou and E. N. Chatzi, Value of structural health information in partially observable stochastic environments, arXiv preprint arXiv:1912.12534, 2020.
- [54] C. P. Andriotis and K. G. Papakonstantinou, Deep reinforcement learning driven inspection and maintenance planning under incomplete information and constraints, arXiv preprint arXiv:2007.01380, 2020.
- [55] Pacific Earthquake Engineering Research Center, PEER Ground Motion Database, [Online]. Available: http://ngawest2.berkeley.edu/.